Exosomal miR-100-5p Inhibits Osteogenesis of BMSCs and Angiogenesis of VECs By Suppressing BMPR2/Smad1/5/9 Signaling Pathway

Wu Yang
The First Affiliated Hospital of Chongqing Medical University
Weiwen Zhu
Sun Yat-sen University First Affiliated Hospital
Yunfei Yang
The First Affiliated Hospital of Chongqing Medical University
Minkang Guo
The First Affiliated Hospital of Chongqing Medical University
Husun Qian
Chongqing Medical University
Weiqian Jiang
The First Affiliated Hospital of Chongqing Medical University
Yu Chen
The First Affiliated Hospital of Chongqing Medical University
Chengjie Lian
The First Affiliated Hospital of Chongqing Medical University
Zijie Xu
The First Affiliated Hospital of Chongqing Medical University
Haobo Bai
The First Affiliated Hospital of Chongqing Medical University
Tingmei Chen
chongqing medical university
Jian Zhang (zhangjian@hospital.cqmu.edu.cn)
The First Affiliated Hospital of Chongqing Medical University https://orcid.org/0000-0003-2908-1935

Research

Keywords: NONFH, Exosomes, osteogenic differentiation, adipocyte differentiation, angiogenesis, miRNAs, BMPR2

Posted Date: January 19th, 2021

DOI: https://doi.org/10.21203/rs.3.rs-149078/v1

Version of Record: A version of this preprint was published at Stem Cell Research & Therapy on July 13th, 2021. See the published version at https://doi.org/10.1186/s13287-021-02438-y.

Exosomal miR-100-5p inhibits osteogenesis of BMSCs and angiogenesis of VECs by suppressing BMPR2/Smad1/5/9 signaling pathway

Wu Yang[1], Weiwen Zhu[4], Yunfei Yang[3], Minkang Guo[1], Husun Qian[2], Weiqian Jiang[1], Yu Chen[1], Chengjie Lian[1], Zijie Xu[1], Haobo Bai[1], Tingmei Chen[2], Jian Zhang[1]
Correspondence: Jian Zhang (zhangjian@hospital.cqmu.edu.cn)
1. Department of Orthopedics, The First Affiliated Hospital of Chongqing Medical University, Chongqing 400016, China
2. Key Laboratory of Diagnostic Medicine Designated by the Ministry of Education, Chongqing Medical University, Chongqing 400016, China
3. Department of Geriatrics, The First Affiliated Hospital of Chongqing Medical University, Chongqing 400016, China
4. Department of Orthopedics, The First Affiliated Hospital of Sun Yat-sen University, Guangzhou 510080, China

Abstract

Background: Non-traumatic osteonecrosis of the femoral head (NONFH) is a common, progressive, and refractory orthopedic disease. We aimed to figure out whether exosomal miRNA from necrotic bone tissues of the non-traumatic osteonecrosis of the femoral head (NONFH) patients are involved in the pathogenesis of NONFH and reveal the underlying mechanisms.
Methods: RT-PCR and western blotting were used to detect the expression of osteogenic, adipogenic and angiogenic markers. ALP staining and Alizarin red s (ARS) staining were used to evaluate osteogenic differentiation of BMSCs. Oil red staining was conducted to test the adipocyte deposition. Tube formation assay was used to study angiogenesis of vascular endothelial cells (VECs). HE staining and IHC staining were used to detect the effect of NONFH-exosomes in vivo. MicroRNA sequencing was conducted to find potential regulators in NONFH-exosomes.
Results: The NONFH-exosomes can lead to NONFH-like impairment on BMSCs, HUVECs and rats. MiR-100-5p was upregulated in NONFH-exosomes and could inhibit osteogenesis of BMSCs and angiogenesis of HUVECs by targeting BMPR2.
Conclusion: The NONFH-exosomal miR-100-5p can lead to NONFH-like damage by targeting BMPR2 and suppressing BMPR2/SMAD1/5/9 signaling pathway, which may be involved in the pathomechanism of non-traumatic osteonecrosis of the femoral head (NONFH).
Key words: NONFH; Exosomes; osteogenic differentiation; adipocyte differentiation; angiogenesis; miRNAs; BMPR2

Introduction

Non-traumatic osteonecrosis of the femoral head (NONFH) is a common, progressive, and refractory orthopedic disease which usually results in substantial loss

of function and inconvenience in daily life of the patients[1-3]. Typically occurs in young adult people aged 30–50, NONFH results in 15,000-20,000 new patients in USA and 100,000-200,000 new patients in China per year[4,5]. Several conservative treatments had been reported in past years, but no pharmacological therapy can completely cure this disease [6]. Therefore, the patients are necessitated to undergo multiple procedures and often culminated with a hip arthroplasty[2, 3]. The difficulties in diagnosis and treatment for this disease mainly result from the unclear underlying mechanisms[7].

The impaired osteogenic differentiation of bone marrow mesenchymal stem cells (BMSCs) and angiogenesis of vascular endothelial cells (VECs) are considered as the main factors leading to the initiation and progression of NONFH[8, 9]. BMSCs, with high proliferative potential and the ability to differentiate into osteoblasts, chondrocytes and adipocytes, are considered as the precursor cells of osteoblasts and play an important role in bone growth, regeneration and reconstruction[10]. In patients with NONFH, BMSCs pools are damaged, and the osteoblasts are significant abnormal[11]. The vascular impairment is indicated by reduced circulating angiogenic cell function, with the migratory function and VEGF protein secretion weakened[12]. In addition, the damage of vascular endothelial cells (VECs) resulted in capillary sparseness, disturbance of the coagulation-fibrinolysis system and thrombi formation in the femoral head, which consequently serious reduced blood supply of the trabecular bone[13].

Exosomes are new mediators to participate in intercellular signal transmission[14]. Recently, these nanoparticles have been reported to be involved in bone and joint diseases, including osteoarthritis, rotator cuff injury, and osteoporosis[15-18]. Exosomes were reported to influence osteogenic differentiation and angiogenesis to regulate bone reconstruction and homeostasis[19-23]. Recent studies revealed that exosomes from mesenchymal stem cells (MSCs) could be used for NONFH in rats[24-27]. However, because of the difficulties in obtaining exosomes in the necrotic bone tissues from NONFH patients, study on NONFH-exosomes had never been reported before. In addition, since cells in the tissue are surrounded by exosomes, BMSCs and VECs treated with exosomes from the necrotic bone tissue in femoral head are similar to the BMSCs and VECs in necrotic region. This helped to study the mechanisms of NONFH and find potential therapeutic targets for NONFH.

MicroRNAs (miRNAs/miRs), a kind of small noncoding RNAs, regulate a large number of genes through binding 3′untranslated regions (3′UTRs) of their target mRNAs and ultimately cleaving the mRNAs or repressing translation of the mRNAs[28-31]. The miRNAs were reported to regulate NONFH by affecting proliferation and differentiation of BMSCs and VECs and apoptosis of osteocytes[32].MiR-100-5p has been reported to serve as an inhibitor of tumor cell growth and migration in various types of cancer such as Nasopharyngeal Carcinoma[33] and prostate cancer[34].

In this study, we strenuously extracted the NONFH-exosomes from necrotic bone tissue in femoral head, explored the effects of NONFH-exosomes on BMSCs, VECs, and rats, and revealed the role of NONFH-exosomes in the initiation and progression

of NONFH as well as the probable causes for the failure of BMSCs transplantation. We also analyzed the microRNA expressions of NONFH-exosomes, studying the effect and the mechanism of the differently expressed miR-100-5p. These findings suggest that NONFH-exosomal miR-100-5p may be a potential molecular target for treating patients with NONFH.

Materials and methods

1. Patients and bone tissues

The study was conducted in accordance with the Declaration of Helsinki. All experiments were approved by the Research Ethics Committee of The Affiliated Hospital of Chongqing Medical University. Finally, 40 NONFH (stage III and IV) patients and 40 femoral neck fracture (FNF) patients who underwent a hip arthroplasty in the First Affiliated Hospital of Chongqing Medical University from December 2018 to October 2020 were recruited. All of these femoral head samples were collected after resection from the femur and immediately divided into two halves with bone knife. A part of the femoral head was rapidly stored in the liquid nitrogen for the next experiments, while the other part of each sample were fixed in 4% paraformaldehyde for the histological study.

Table1 Demographics data of the study groups

group	gender (male/female)	side (right/left)	age (years)	BMI (kg/m^2)	Acro stage	Yield of exosomes (10^{10}/g)
NONFH	24/16	21/19	63.95±6.11	22.84±2.71	stage III (n=19) stage IV (n=21)	2.89±1.15
FNF	22/18	16/24	64.08±5.53	22.81±2.01		1.26±0.46

Note: Data are presented as mean ± standard error of mean (SEM). “NONFH” represents the group of non-traumatic osteonecrosis of the femoral head. “BMI” means body mass index.

2. Extraction of exosomes from NONFH and FNF bone tissues

Based on the methods previously reported, exosomes were extracted from bone tissue after homogenized by grinding with liquid nitrogen[7]. The isolation and purification followed the multistep ultracentrifugation process. In briefly, the homogenate was centrifuged at 300g for 10 min, 1,500 g for 10 min and 10,000 g for 30 min. Next, the supernatant was centrifuged at 100,000 g for 2×70 min. The centrifugal was performed at 4℃. After every centrifugal, the supernatant was transferred into a new centrifuge tube. Meanwhile, the solution without exosomes was also collected. Finally, the exosomes were washed by PBS and filtered with a 0.22 um filter, and then stored in 100 μL PBS at -80 °C. Some exosome pellets were lysed in RIPA and PMSF lysis buffer (RIPA:PMSF = 100:1) to extract proteins for western blotting analysis.

3. Characterization of exosomes

The size distribution of exosomes was measured by nanoparticle tracking analysis (NTA) using a NanoFCM N30E particle size analyzer. The data were processed with the Zeta View software. The morphology of FNF-exosomes and NONFH-exosomes

were visualized by a Hitachi HT-7700 transmission electron microscope (TEM). The exosomal biomarkers CD9, CD63, Alix and TSG101 were analyzed by western blotting. The Calnexin also was selected to be a positive control. The ultra-centrifuged supernatant mentioned above was used as negative control (NC) in western blotting.

4. Cells culture and transfection

The bone marrow mesenchymal stem cells (BMSCs) and Human umbilical vein endothelial cells (HUVECs) were purchased in Otwo Biotech(Guangdong, China). Cells were in Dulbecco's modified eagle medium high glucose(HyClone Laboratories Inc., Beijing, China) suppled with 10% fetal bovine serum (Gibco, UK), 100 U/mL penicillin and 100 μg/mL streptomycin (NCM, China) at 37℃ and 5%CO_2. The medium was changed every 3 days. The both concentration of FNF-exosomes and NONFH-exosomes added into cells was 60 μg/ mL.

The negative control (NC), agomiR-100-5p, antagomir-100-5p and siBMPR2 (Genpharma, Shanghai, China) were transfected into cells with Endofectin^{TM}-MAX （GeneCopoeia,USA）according to manufacturer's guidelines. The working concentration of agomiR-100-5p was100 nM, and those of antagomiR-100-5p, NC and siBMPR2 were 200 nM.

5. Cell uptake of exosomes

The exosomes were stained by PKH67 kit (BestBio, China) according to the protocol of the manufacturer. The labeled exosomes were dissolved in the sterile PBS. The BMSCs and HUVECs were treated by exosomes labeled by PKH67 and cultured in serum-free medium for 24 hours. Then, the cells were washed by PBS and subsequently fixed by 4% paraformaldehyde for 30min. Afterwards, the nuclei were stained by Diaminophenyl indole (DAPI) for 10min at room temperature and next the redundant dye was washed off. At last, the cells were observed under a fluorescence microscopy (Leica, UK).

6. Osteogenic differentiation, Alkaline phosphatase staining and Alizarin red S staining

The BMSCs were inoculated in 24-well plates. When the confluence point of cells reached 80%, the medium was changed as the osteogenic differentiation medium (Cyagen, USA). Alkaline phosphatase staining and Alizarin red staining were used to evaluate the level of osteogenic differentiation. After cultured in osteogenic differentiation for 7 days, alkaline phosphatase (ALP) staining was conducted according to instruction of the manufacturer (Beyotime, China). After cultured in osteogenic differentiation for 3 weeks, the BMSCs were fixed, stained and cleared according to the instructions of the Alizarin Red S staining kit (Solarbio, China).

7. Adipocyte differentiation and oil staining

When the confluence point of cells reached 100%, the medium was changed as the adipocyte differentiation medium (Cyagen, USA). After cultured in adipocyte differentiation medium for 4 weeks, the BMSCs were stained with Oil red saining according to instruction of the manufacturer (Solarbio, China).

8. Wound healing assay

Cell migration of BMSCs and HUVECs were detected by the wound healing assay. The cells were plated on six-well plates with the concentration of 8×10^5 cells/well.

When the confluence was more than 95–100%, the monolayer was scratched using a 10 μL sterile pipette tip and then cultured with the sterile serum-free medium. Wound width both at baseline, the images of cells in HUVECs at 36 h and BMSCs at 48 h were obtained via optical microscopy (Leica, Germany) to evaluate the migration ability of cells in each group.

9. Tube Formation Assay

To evaluate the effect of PBS, FNF-exosomes and NONFH-exosomes on HUVEC tube formation, HUVECs were seeded at 40,000 cells/well in Matrigel-coated 48-well plates. The cells were cultured in culture medium supplemented with FNF-exosomes (50 μg/mL), NONFH (50 μg/mL), or PBS at the same volume. Six hours later, tube formation was observed under an optical microscope.

10. RNA extraction

Total RNA was extracted according to the operation manual of simply P total RNA extraction kit (BioFlux, China). MiRNA was extracted according to the operation manual of Biospin miRNA Extraction kit（BioFlux，China）. Finally, Biodrop Ulite (UK) was used to detect the RNA concentration.

11. MiRNA sequencing

The high-throughput sequencing service was provided by Novogene (Beijing, China). Briefly, Sequencing libraries were generated using NEBNext® Multiplex Small RNA Library Prep Set for Illumina® (NEB, USA.) following manufacturer's recommendations and index codes were added to attribute sequences to each sample. The clustering of the index-coded samples was performed on a cBot Cluster Generation System using TruSeq SR Cluster Kit v3-cBot-HS (Illumia) according to the manufacturer's instructions. Differential expression analysis of two groups was performed using the DESeq R package (1.8.3). T with P value≥0.05. Gene Ontology (GO) enrichment and KEGG enrichment analysis were used on the target gene candidates of differentially expressed miRNAs ("target gene candidates" in the following).

12. Real-time quantitative PCR

The mRNAs were reverse transcripted into cDNA using the PrimeScriptTM Reagent Kit with gDNA Eraser (TaKaRa, Japan). A 20 μL system was used for real-time quantitative PCR reaction, and 4 secondary pores were set. The relative expression levels of mRNAs were standardized with β-actin. The relative expression of miRNA and mRNA was standardized by u6 and -actin. The primers were showed in Table 2.

Table2 Primer sequence

gene name	Primer sequence
ALP	F CACGGCGTCCATGAGCAGAAC
	R CAGGCACAGTGGTCAAGGTTGG
COL1A1	F TGTTGGTCCTGCTGGCAAGAATG
	R GTCACCTTGTTCGCCTGTCTCAC
RUNX2	F TCCGCCACCACTCACTACCAC
	R GGAACTGATAGGACGCTGACGAAG

β-actin	F TGGCTCTAACAGTCCGCCTAG
	R AGTGCGACGTGG ACATCCG
OCN	F GGACCCTCTCTCTGCTCACTCTG
	R ACCTTACTGCCCTCCTGCTTGG
PPARγ	F CCATCGAGGACATCCAAGACAACC
	R GTGCTCTGTGACAATCTGCCTGAG
VEGFA	F GCCTTGCCTTGCTGCTCTACC
	R CTTCGTGATGATTCTGCCCTCCTC
FGF2	F GAAGAGCGACCCTCACATCAAGC
	R CCAGGTAACGGTTAGCACACACTC
OPN	F CCAGCCAAGGACCAACTACA
	R GCTGGCAGTGAAGGACTCAT
miR-100-5p	F GGAACCCGTAGATCCGAACTTGTG
	R AACGCTTCACGAATTTGCGT
U6	F CTCGCTTCGGCAGCACA
	R AACGCTTCACGAATTTGCGT

13. The extraction of proteins and Western blot

Protein lysate (RIPA, Beyotime, China) and protease inhibitor (PMSF, NCM, China) were used to extract protein. The protein concentration of the samples was detected by BCA protein concentration determination kit (Beyotime, China). 30 μg protein was loaded into each lane, separated with 10% SDS-PAGE separation gel (Wanlei, China) at 80 V for 30 minutes and at 120V for 60 minutes, then transferred to PVDF membrane (Millipore, USA), and closed with rapid blocking solution (NCM, China). Then, the protein bands were incubated in primary antibody at 4℃ overnight. The primary antibodies β-actin, Alix, CD63, CD9, Calnexin, PPARγ, Runx2, VEGFA, OPN, Collagen1 were purchased from WanleiBio. ALP and TSG101 were purchased from Abcam. FGF2 was purchased from Sabbiotech. OCN and BMPR2 were purchased from Affinity. SMAD1/5/9 and p-SMAD1/5/9 were purchased from ZenBio. After the application, the protein bands were washed with TBST for three times, and then incubated with secondary antibodies (Goat anti-rabbit, 1:8,000, Proteintech, China) for 1 hour. After dressing, TBST was used for three times, and finally the protein was detected with Zen-Bio (Chengdu, China) reagent.

14. Dual luciferase reporter assay

The relationship between the BMPR2 and miR-100-5p was predicted by the bioinformatics database Targetscan 7.2 (www.targetscan.org). Next, human embryonic kidney (HEK)-293T cells were cultured in DMEM containing 10% FBS at 37◦C with 5% CO2. A cDNA fragment containing 3' -untranslated region (UTR) of BMPR2 (binding site to miR-100-5p) was inserted into the pmirGLO vector. A cDNA fragment of BMPR2 3'-UTR with a binding site mutation was constructed with DNA point mutation. It was then inserted into the pmirGLO vector and confirmed to be correct by sequencing. The pmirGLO- BMPR2 or pmirGLO-mut BMPR2

recombinant vector was co-transfected into HEK-293T cells with agomiR-100-5p or miR-NC. After incubation for 48 h, cells were collected and lysed. Then, 100 μl lysate wasmixed with 100 μl Renilla luciferase assay working solution and subject to Renilla luciferase activity measurement. Meanwhile, 100 μl lysate was mixed with 100 μl firefly luciferase detection reagent for detecting the firefly luciferase activity. Subsequently, a multimode microplate reader SpectraMaxM5 (interval: 2 s; duration: 10 s) was employed to determine the activity of Renilla luciferase and firefly luciferase, respectively.

15. Animal study

All experimental and animal care procedures were approved by the the Research Ethics Committee of The Affiliated Hospital of Chongqing Medical University and performed in accordance with the guidelines of the National Institutes of Health Guidelines for the Care and Use of Laboratory Animals. A total of 30 female SD rats (8-week old, 180-200g) were enrolled in this study and randomly divided into 3 groups: the PBS rats (n=10), FNF-exosomes rats (n=10), and NONFH-exosomes rats (n=10) respectively injected with PBS, FNF-exosomes, and NONFH-exosomes. PBS, FNF-exosomes, and NONFH-exosomes were injected into rats once every other day for 8 weeks via tail vein. After 8-week injection, all rats were sacrificed to harvest the femoral heads. A micro-CT (Skyscan1174 X-Ray Microtomograph, Bruker, Belgium) was used to scan the rat femoral heads. After scanning, software N-Recon was used for 3-demetional reconstruction of the femoral heads and software CT-AN was used to analyze the osteogenic parameters including BV/TV (bone volume per tissue volume), Tb.Sp (trabecular separation), Tb.Th (trabecular thickness) and Tb.N (trabecular number).

16. Histological analyses and immunohistochemistry (IHC)

The collected femoral heads were fixed with 4%paraformaldehyde for a week and decalcified with EDTA decalcifying solution. The samples were embedded in paraffin and cut into 5 μm sections, deparaffinised in xylene, rehydrated in a graded series of ethanol solutions, and rinsed in distilled water. HE staining was performed for histological observation. The osteogenesis of bone tissue around the femoral heads was assessed by IHC staining.

17. Statistical analysis

Statistical analyses were performed using GraphPad PRISM8.0. For all data, normality and homogeneity of variance were detected. All of the measurement data were expressed as mean ± standard error of mean. For the comparison between two groups, the Student's T-test method was used, while for the comparison between multiple groups, one-way ANOVA and Tukey test method were used. P values ≤ 0.05 was considered statistically significant.

Results

Characteristics of NONFH samples, FNF samples, NONFH-exosomes and FNF-exosomes

The hip joint X-ray of the NONFH group shows the necrosis, collapse and deformation of the femoral head (Fig.1A). Figure1B shows sectional images of

femoral head specimens from FNF group and NONFH group. The HE stainings showed normal bone trabecula in FNF group and collapse, disorder, fracture and necrosis of trabecula in NONFH group (Fig.1C). The expressions of CD31 (Fig. 1D) and RUNX2 (Fig. 1E) were notably declined in necrotic bone tissue. The results of western blotting showed down-regulations of osteogenic and angiogenic markers (ALP, OPN, and FGF2) and up-regulation of adipogenic marker-PPARγ (Fig.1F).

To characterize the purified exosomes fractions, TEM, NTA, and the exosomal markers analysis were conducted. The transmission electron microscope (TEM) indicates typical intact spherical homogeneous morphology of FNF-exosomes and NONFH-exosomes with diameters about 100 nm (Fig.1G-H). The results from NTA showed diameter distribution with an average dimension of 71.83±12.75 nm in FNF-exosomes and 70.29±11.88 nm in NONFH-exosomes (Fig. 1 I-J). Figure 1K shows the expression of the exosome markers CD63, CD9, Alix, Calnexin and TSG-101 in exosomes and supernatant. The uptake assay showed the exosomes could be endocytosed by BMSCs (Fig.1L) and HUVECs (Fig. 1M). These data indicate that exosomes were successfully isolated from normal and necrotic bone tissues and can be absorbed by BMSCs and HUVECs.

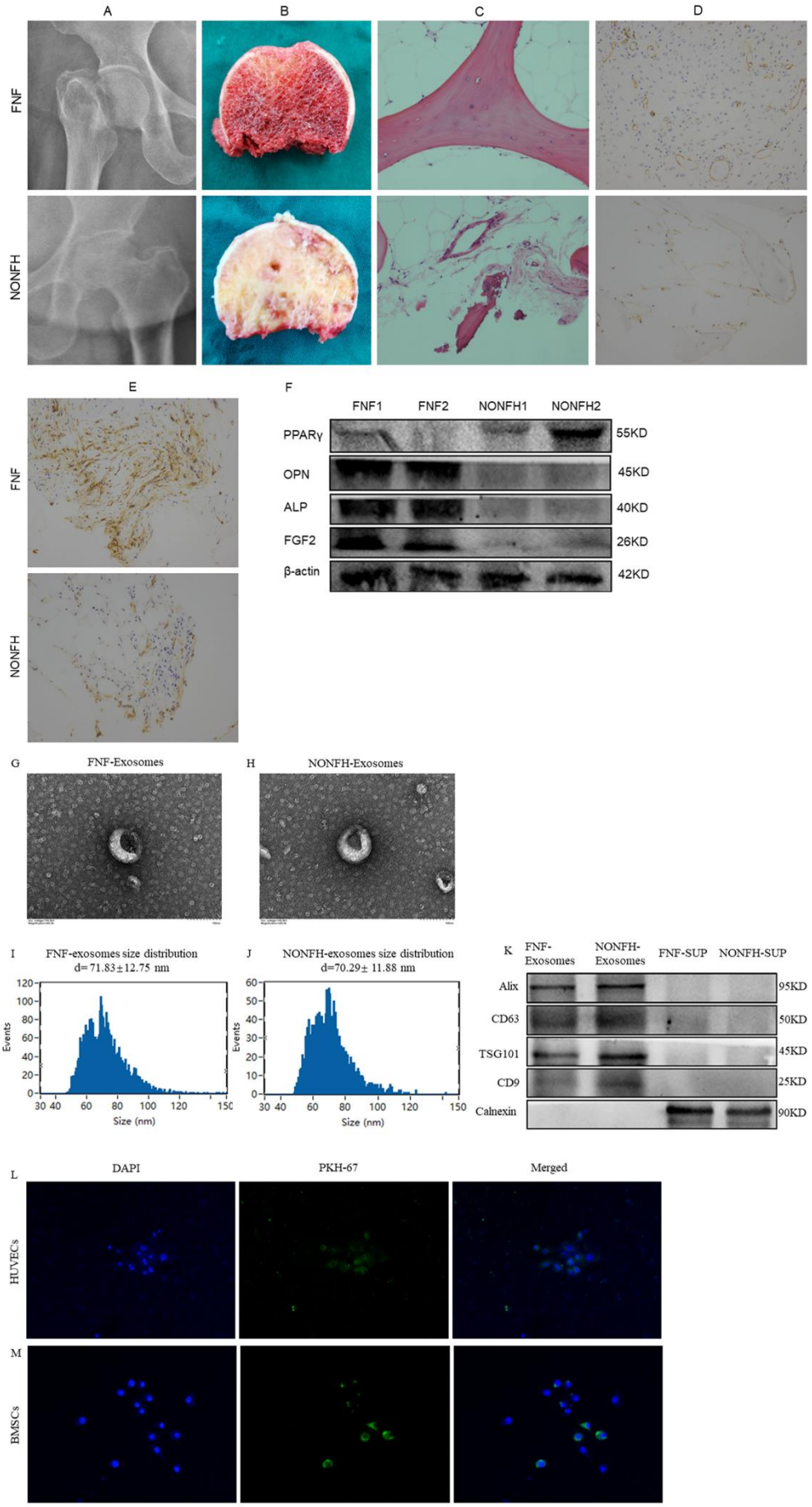
A
B
C
D
FNF
NONFH
E
FNF
NONFH
F
FNF1
FNF2
NONFH1
NONFH2
PPARγ
55KD
OPN
45KD
ALP
40KD
FGF2
26KD
β-actin
42KD
G
FNF-Exosomes
H
NONFH-Exosomes
I
FNF-exosomes size distribution
d= 71.83±12.75 nm
J
NONFH-exosomes size distribution
d=70.29± 11.88 nm
Events
Size (nm)
K
FNF-Exosomes
NONFH-Exosomes
FNF-SUP
NONFH-SUP
Alix
95KD
CD63
50KD
TSG101
45KD
CD9
25KD
Calnexin
90KD
L
DAPI
PKH-67
Merged
HUVECs
M
BMSCs

Figure. 1 Characteristics of NONFH samples, FNF samples, NONFH-exosomes and FNF-exosomes. A-C Representative X-rays (A), sectional images (B), and HE stainings (C) of femoral heads from FNF and NONFH patients (×100). **D-E** IHC stainings of CD31 (D) and RUNX2 (E) were conducted in femoral heads of FNF and NONFH patients (×200). **F** The expressions of PPARγ, OPN, ALP, FGF2 were measured by western blotting. **G-H** TEM images displayed the double membrane and discoid shape of FNF-exosomes (G) and NONFH-exosomes (H) (scale bar=100 nm). **I-J** Particle size distributions of FNF-exosomes (I) and NONFH-exosomes (J) were measured by NTA. **K** The expressions of CD63, CD9, Alix, Calnexin and TSG101 in FNF-exosomes, NONFH-exosomes, and the FNF-supernatants (FNF-SUP) and NONFH-supernatants (NONFH-SUP) were examined by western blotting. **F, G** Observation of PKH-67-labeled exosomes were uptaken into BMSCs and HUVECs under the fluorescence microscopy (×200, scale bar=50 μm), where green (PKH-67) indicates exosomes and blue (DAPI) indicates BMSCs and HUVECs.

NONFH-exosomes inhibited osteogenesis of BMSCs and angiogenesis of VECs , promoting adipogenesis of BMSCs

To investigate the effect of FNF-exosomes and NONFH-exosomes on osteogenesis and adipogenesis of BMSCs, we examined the osteogenic and adipogenic markers, including OCN, OPN, ALP, RUNX2, Collagen 1, and PPARγ, in BMSCs treated with PBS, FNF-exosomes, or NONFH-exosomes for 7 days. The results of western blotting and RT-PCR showed that the expressions of osteogenic markers were declined in NONFH-exosomes group, while the expression of PPARγ was increased (Fig. 2A-B). In addition, ALP activity assay and ALP staining demonstrated the suppressing effect of NONFH-exosomes on ALP activity of BMSCs (Fig.2C-D). Alizarin red S staining also exhibited the significant decrease of calcium deposition on the surface of BMSCs in NONFH-exosomes group (Fig. 2E). The oil red staining showed that NONFH-exosomes promoted the formation of lipid droplet in BMSCs (Fig. 2F). These data indicate that NONFH-exosomes could inhibit the osteogenic differentiation of BMSCs, accompanied with an augment in the adipocyte differentiation of BMSCs.

Next, we measured the angiogenesis ability of HUVECs treated with NONFH-exosomes by employing RT-PCR, WB and a tube formation assay. The figure 3G and figure 2H showed the down-regulation of VEGFA and FGF2 in HUVECs treated with NONFH-exosomes. The tube formation assay showed that the formatted tubes of HUVECs were significantly decreased in NONFH-exosomes group (Fig. 2I). These data indicated that NONFH-exosomes influenced angiogenesis of HUVECs.

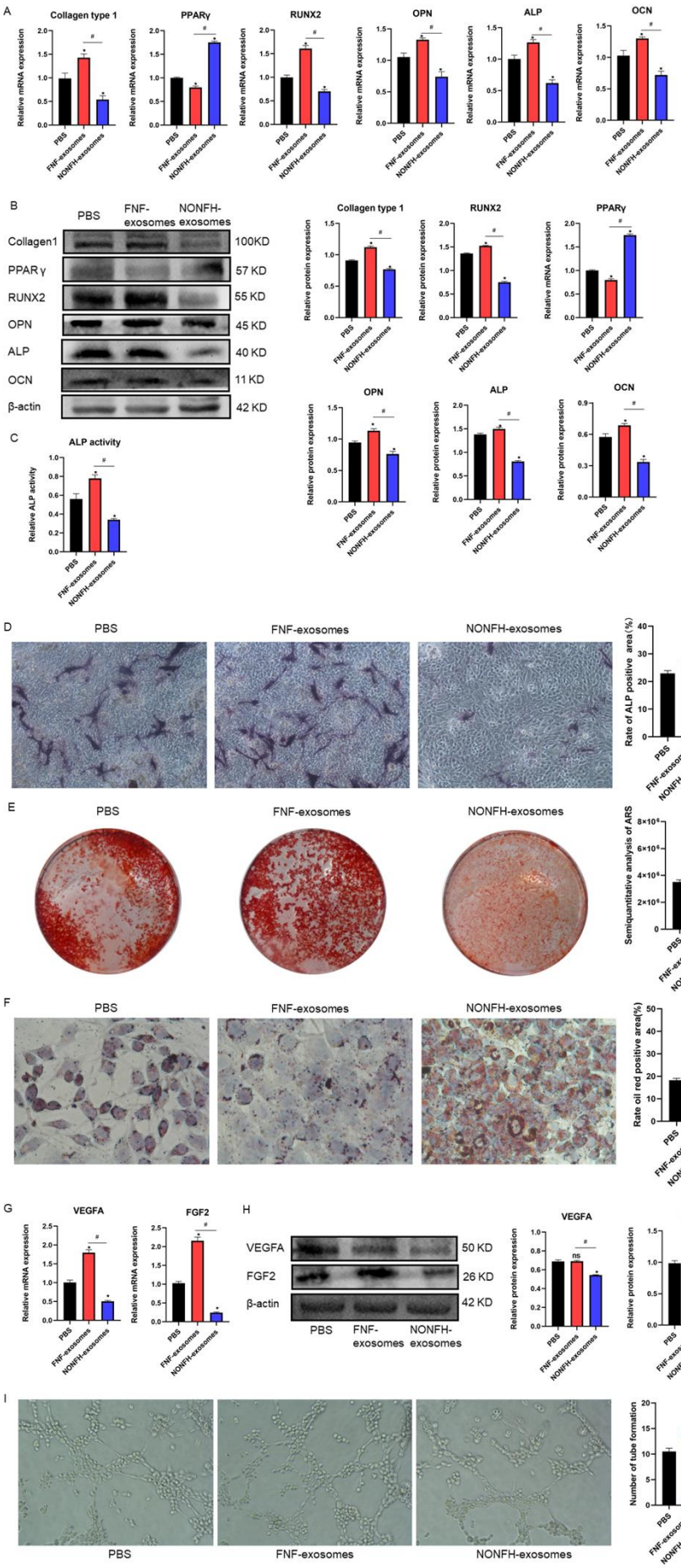
A
Collagen type 1
PPARγ
RUNX2
OPN
ALP
OCN
Relative mRNA expression
PBS
FNF-exosomes
NONFH-exosomes
B
PBS
FNF-exosomes
NONFH-exosomes
Collagen1
PPARγ
RUNX2
OPN
ALP
OCN
β-actin
100KD
57 KD
55 KD
45 KD
40 KD
11 KD
42 KD
Relative protein expression
Relative mRNA expression
C
ALP activity
Relative ALP activity
D
PBS
FNF-exosomes
NONFH-exosomes
Rate of ALP positive area(%)
E
Semiquantitative analysis of ARS
F
Rate oil red positive area(%)
G
VEGFA
FGF2
H
50 KD
26 KD
42 KD
ns
I
Number of tube formation

Figure. 2 NONFH-exosomes inhibited osteogenic differentiation and promoted adipogenic differentiation of BMSCs. A-B The expressions of Collagen1, OCN, RUNX2, ALP, OPN and PPARγ were measured by RT-PCR (A) and WB (B) in BMSCs treated with PBS, FNF-exosomes, or NONFH-exosomes. **C-D** ALP activity and ALP staining of BMSCs . (×100). **E** Alizarin red staining of BMSCs. **F** Oil red staining of BMSCs (×400). **G-H** The expressions of VEGFA, FGF2 were measured by RT-PCR (G) and western blotting (H). **I** Tube formation assay of HUVECsl. *P <0.05, versus PBS group; #P < 0.05, versus FNF-exosomes group. All data were expressed as mean ± SEM.

NONFH-exosomes inhibited the migration ability of BMSCs and HUVECs

Next, we conducted wound healing assays to investigate the effects of NONFH-exosomes on the migration ability of BMSCs and HUVECs. The pictures photographed at 0 h and the terminal point 48 h of BMSCs showed the migration ability of BMSCs was suppressed by NONFH-exosomes and promoted by FNH-exosomes (Fig. 3A-B). In addition, the images saved at 0 h and 36 h indicated the migration of HUVECs was also inhibited in NONFH-exosomes group (Fig. 3C-D). These results showed that migratory distances of BMSCs and HUVECs in NONFH-exosomes group were decreased.

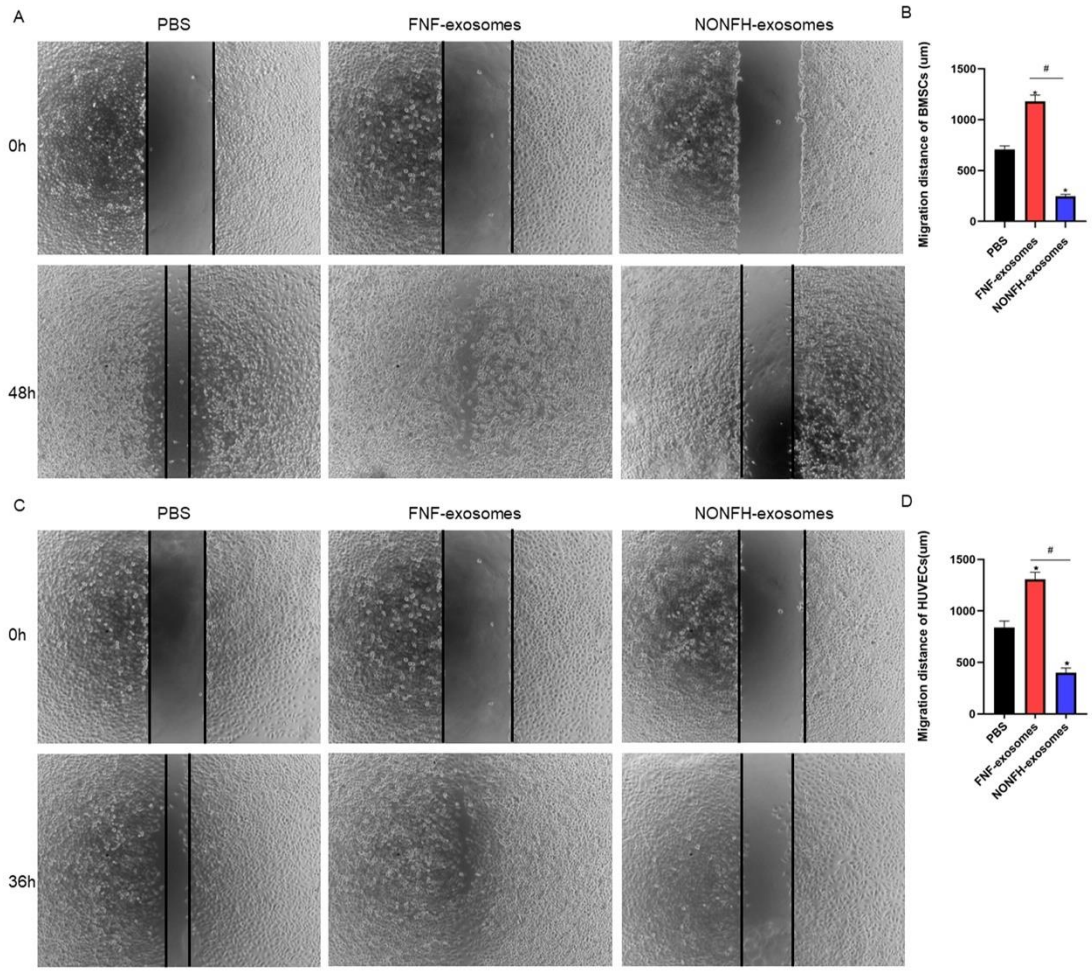

Figure. 3 NONFH-exosomes inhibited the migration ability of BMSCs and HUVECs. A-B Wound healing assay of BMSCs (A) and its quantitative analysis (B). **C-D** Wound healing assay of HUVECs

(C) and its quantitative analysis (D). *P <0.05, versus PBS group; #P < 0.05, versus FNF-exosomes group. All data were expressed as mean ± SEM.

NONFH-exosomes could lead to NONFH-like damage on rats

Finally, the NONFH-exosomes, FNF-exosomes, or PBS were injected into rats via tail vein to explore the effects of NONFH-exosomes in vivo. The micro-CT scanning results suggested that about 60% rats in NONFH-exosomes group had bone tissue changes, including subchondral bone lesion, collapse, and malformed shape of the femoral head (Fig. 4A). Qualitative analyses of all the micro-CT parameters showed that BV/TV, Tb. Th and Tb. N were decreased with the augment of Tb. Sp in the rats of NONFH-exosomes group (Fig. 4B). The HE staining revealed the NONFH-like damage in the NONFH-exosomes group, including subchondral bone lesion, more marrow cavity and sparser trabecula (Fig. 4C-D). Next, the IHC staining showed the reduction of RUNX2 and VEGFA (Fig.4E). The results of western blotting showed that the expressions of Collagen1, VEGFA, FGF2, RUNX2, OPN, ALP and OCN were down-regulated in the rats of NONFH-exosomes group, while the expression of PPARγ was up-regulated (Fig.4F-G). These data indicate that NONFH-exosomes induced the NONFH-like damage with the decline of osteogenesis and angiogenesis and augment of adipogenesis in vivo.

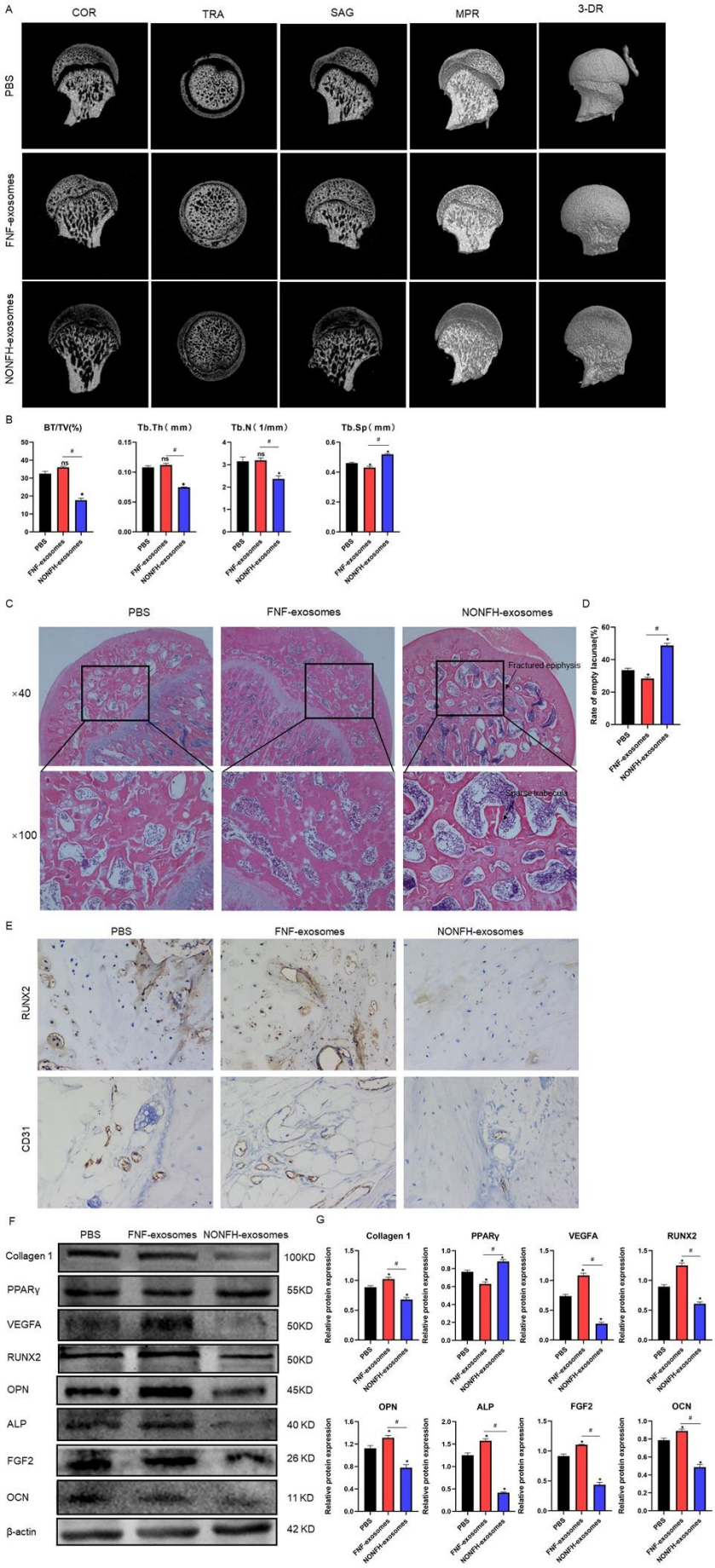
A
COR
TRA
SAG
MPR
3-DR
PBS
FNF-exosomes
NONFH-exosomes
B
BT/TV(%)
Tb.Th（mm）
Tb.N（1/mm）
Tb.Sp（mm）
ns
#
*
C
PBS
FNF-exosomes
NONFH-exosomes
×40
×100
Fractured epiphysis
Sparse trabecula
D
Rate of empty lacunae(%)
E
RUNX2
CD31
F
Collagen 1
PPARγ
VEGFA
RUNX2
OPN
ALP
FGF2
OCN
β-actin
100KD
55KD
50KD
50KD
45KD
40 KD
26 KD
11 KD
42 KD
G
Relative protein expression

Fig. 4 NONFH-exosomes could lead to NONFH-like damage on rats. A COR, TRA, SAG, MPR, and 3-DR images of rat femoral heads. COR, coronal; TRA, transverse; SAG, sagittal; MPR, multiplanar reconstruction; 3-DR, three-dimensional reconstruction. **B** Quantitative analysis of micro-CT scanning. BV/TV, bone volume per tissue volume; Tb.N, trabecular number; Tb.Sp, trabecular separation; Tb.Th, Trabecular thickness. **C** HE stainings of the femoral heads. **D** Quantitative analysis of marrow cavity. **E** The expression of RUNX2, CD31 in the femoral head of rats were measured by IHC staining($P < 0.05$). **F** Western blot was used to detect the expression of Collagen1, VEGFA, FGF2, RUNX2, OPN, PPARγ, ALP, and OCN in femoral heads of rats. **G** Quantitative analysis of WB. *$P < 0.05$, versus PBS group; #$P < 0.05$, versus FNF-exosomes group. All data were expressed as mean ± SEM.

MiR-100-5p was up-regulated in NONFH-exosomes

To investigate if the expressions of miRNAs were different between NONFH-exosomes and FNF-exosomes, microRNA sequencing was performed. We analyzed differentially abundant miRNAs following the criteria of *P-value* < 0.05. Differentially abundant miRNAs between NONFH-exosomes and FNF-exosomes were visualized using Volcano plot (Fig.5A) and heatmap (Fig.5B). A total of 30 differentially expressed miRNAs were identified, including 12 up-regulated miRNAs and 18 downregulated miRNAs. The results of GO enrichment and KEGG pathway enrichment analysis were separately displayed in (Fig. 5C-D). RT-PCR was further used to measure the expression of miR-100-5p and the result was similar to the results of microRNA sequencing (Fig. 5E).

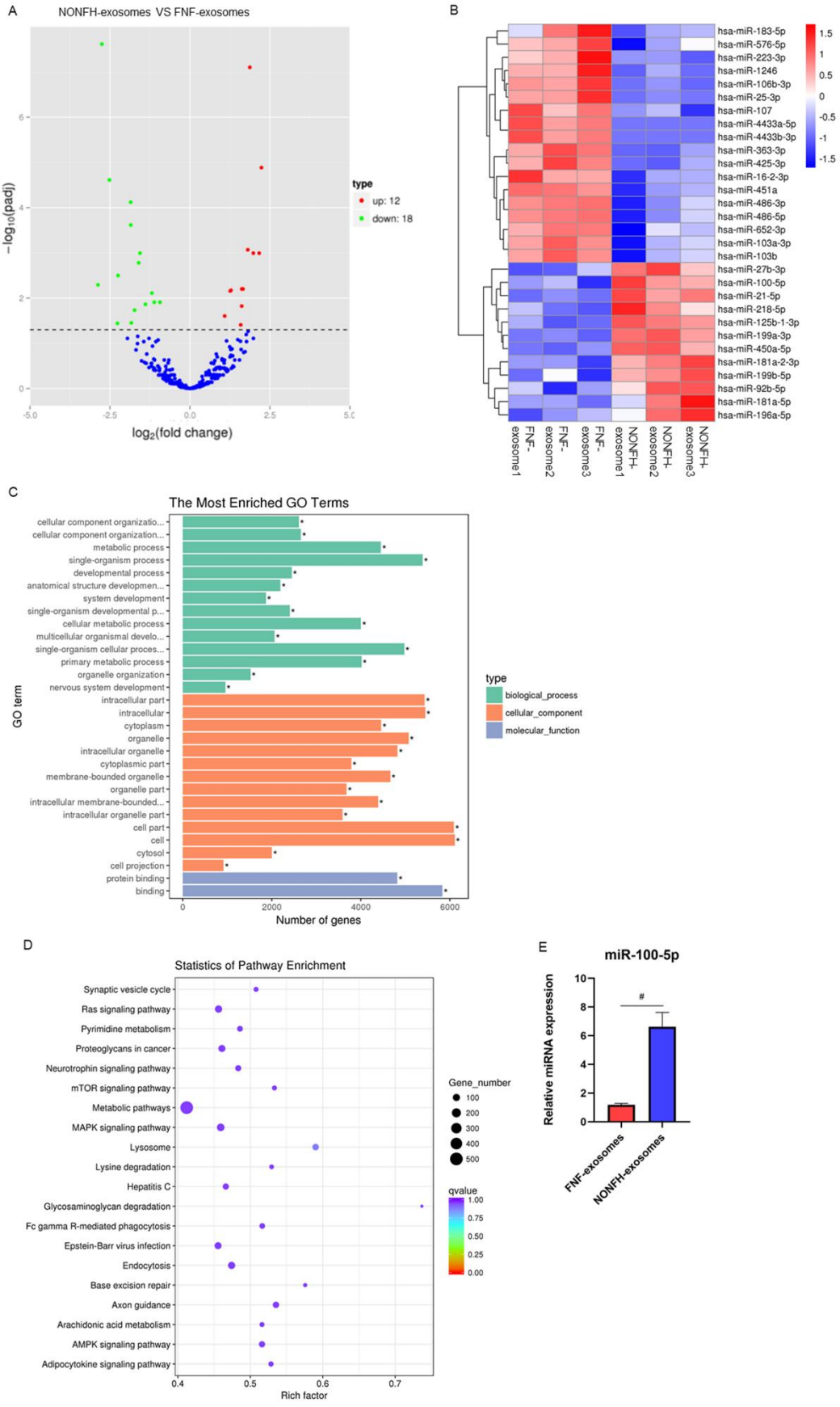

Figure. 5 MiR-100-5p was up-regulated in NONFH-exosomes. A Volcano map of the miRNA

sequencing. **B** Heatmap of the miRNA sequencing (B). **C** GO enrichment. **D** KEGG pathway enrichment. E RT-PCR was used to detect the expression of miR-100-5p in FNF-exosomes and NONFH-exosomes. #P < 0.05, versus FNF-exosomes group. All data were expressed as mean ± SEM.

MiR-100-5p inhibited osteogenesis of BMSCs and angiogenesis of HUVECs, promoting adipogenesis of BMSCs

As the results of the miRNA sequenceing and RT-qPCR showed that the miR-100-5p was up-regulated in NONFH-exosomes, we studied the effects of miR-100-5p on BMSCs and HUVECs. We found that the transfection of agomiR-100-5p and antagomiR-100-5p could separately increase and decrease the expression of miR-100-5p in BMSCs and HUVECs (Fig.6A, C). The results of western blotting showed that the expressions of OCN, RUNX2, ALP and Collagen1 were significantly reduced in BMSCs transfected with agomiR-100-5p with the augment of PPARγ (Fig. 6B). The ALP staining showed that the ALP activity of BMSCs was inhibited in agomiR-100-5p group (Fig. 6D). The ARS staining showed the mineralization of BMSCs was reduced in agomiR-100-5p group (Fig. 6E). The results of oil staining showed the formation of lipid droplets was promoted in agomiR-100-5p BMSCs group (Fig.6F). The results of western blotting showed the expressions VEGFA and FGF2 were significantly decreased in HUVECs transfected with agomiR-100-5p (Fig.6G). Next, we conducted tube formation assays and the results showed that agomiR-100-5p inhibited tube formation of HUVECs (Fig.6H).

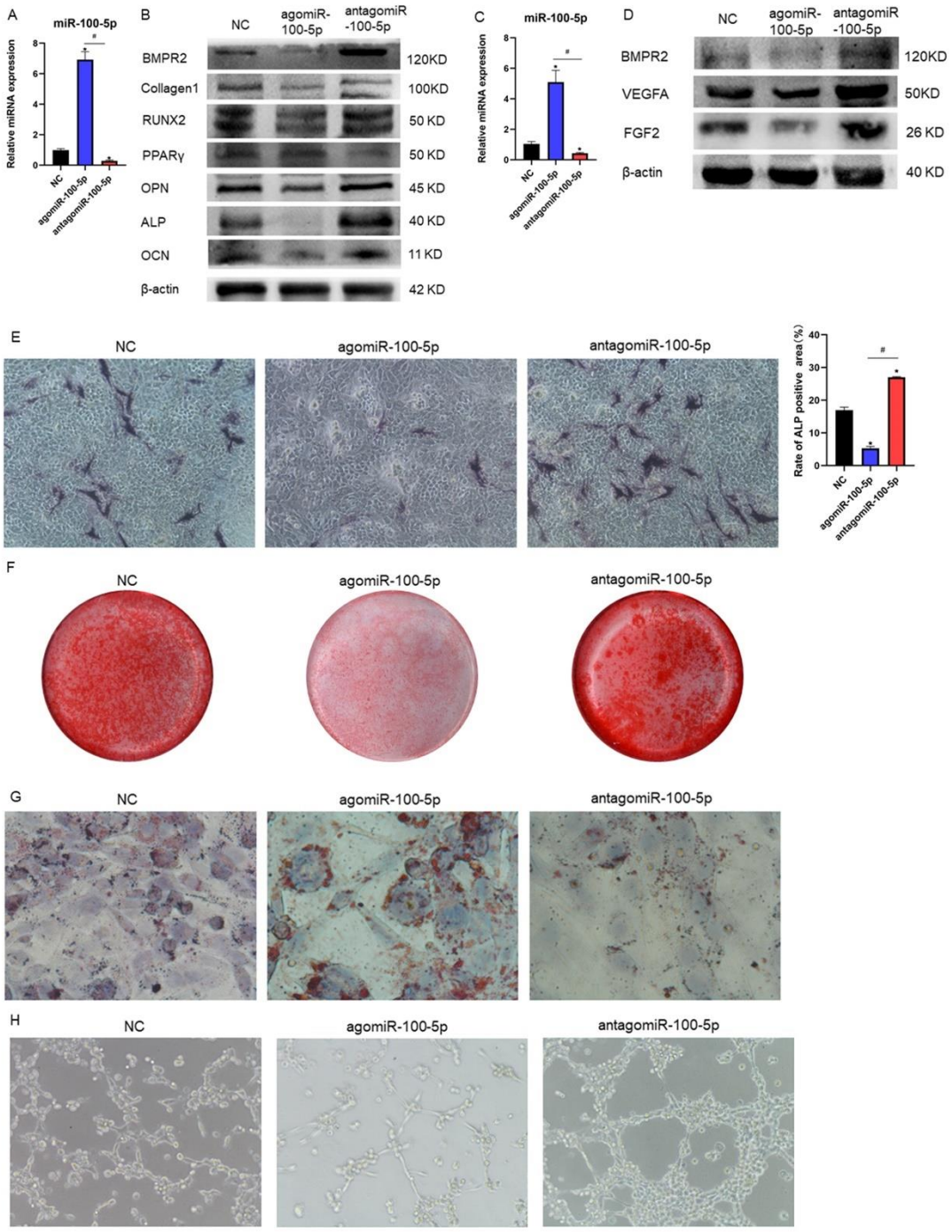

Figure. 6 MiR-100-5p inhibited osteogenesis of BMSCs and angiogenesis of HUVECs, promoting adipogenesis of BMSCs. A The expressions of miR-100-5p in BMSCs transfected with NC, agomiR-100-5p and antagomir-100-5p.**B** The expressions of BMPR2, Collagen1, OCN, RUNX2, ALP, OPN and PPARγ were measured using WB in BMSCs. **C** The expressions of miR-100-5p in HUVECs transfected with NC, agomiR-100-5p and antagomir-100-5p. **D** The expressions of BMPR2, FGF2 and VEGFA were measured using WB in HUVECs. **E** ALP staining of BMSCs. (×100). **F** Alizarin red staining of BMSCs after cultured in ODM for 14 days. **G** Oil red staining of BMSCs (×400). **H** Tube formation assay of HUVECs. *P <0.05, versus NC group; #P < 0.05, versus agomiR-100-5p group. All data were expressed as mean ± SEM.

MiR-100-5p inhibits osteogenesis of BMSCs and angiogenesis of HUVECs by targeting BMPR2 and inhibiting BMPR2/smad1/5/9 pathway.

We predicted the target genes using targetscan 7.2. We found that there was a binding side between miR-100-5p and BMPR2 (Fig. 7A). This finding was further confirmed by a dual luciferase reporter assay (Fig. 7B) and western blotting (Fig. 6 B, D), the results of which showed that overexpression of miR-100-5p significantly suppressed the luciferase activity of 3'-UTR in the wild-type compared with the miR-NC group, whereas no differences in luciferase activity of 3'-UTR was observed in the mutant-type. The above results confirmed that BMPR2 was the target gene of miR-100-5p.

To further investigate the function of BMPR2, we silenced the expression of BMPR2 to evaluate changes in differentiation of BMSCs and HUVECs. The silence of BMPR2 significantly reduced osteogenic differentiation, evidenced through decreased osteogenic markers (Fig. 7 C), diminished ALP activity (Fig.7E), and decreased mineralization capacity (Fig.7F) with the augments of adipogenic marker and lipid droplets in BMSCs (Fig.7 C, G). The down-regulation of miR-100-5p (antagomiR-100-5p) partly rescued the negative effect of siBMPR2 on osteogenesis and the positive effect on adipogenesis of BMSCs. The silence of BMPR2 in HUVECs significantly reduced the expressions of FGF2 and VEGFA and the number of formatted tubes (Fig.7 B, H). From the KEGG database, we found that BMPR2 were associated with BMP-SMAD pathway. According to the previous study, BMP-SMAD signaling was significantly associated with osteogenesis and angiogenesis[35-36]. We next detected BMPR2, SMAD1/5/9 and phosphorylated SMAD1/5/9 (p-SMAD1/5/9) in BMSCs and HUVECs (Fig. 9 A, B). It was obvious that siBMPR2 influenced the expression of these proteins in BMSCs and HUVECs. The silence of BMPR2 suppressed the osteogenesis of BMSCs and angiogenesis of HUVECs via inactivating BMPR2/SMAD1/5/9 pathway. The suppression of miR-100-5p could partly rescue the suppression of osteogenesis of BMSCs and angiogenesis of HUVECs caused by siBMPR2. Taken together, these data suggest that the BMPR2/SMAD1/5/9 pathway is involved in the osteogenesis and angiogenesis through interaction with miR-100-5p.

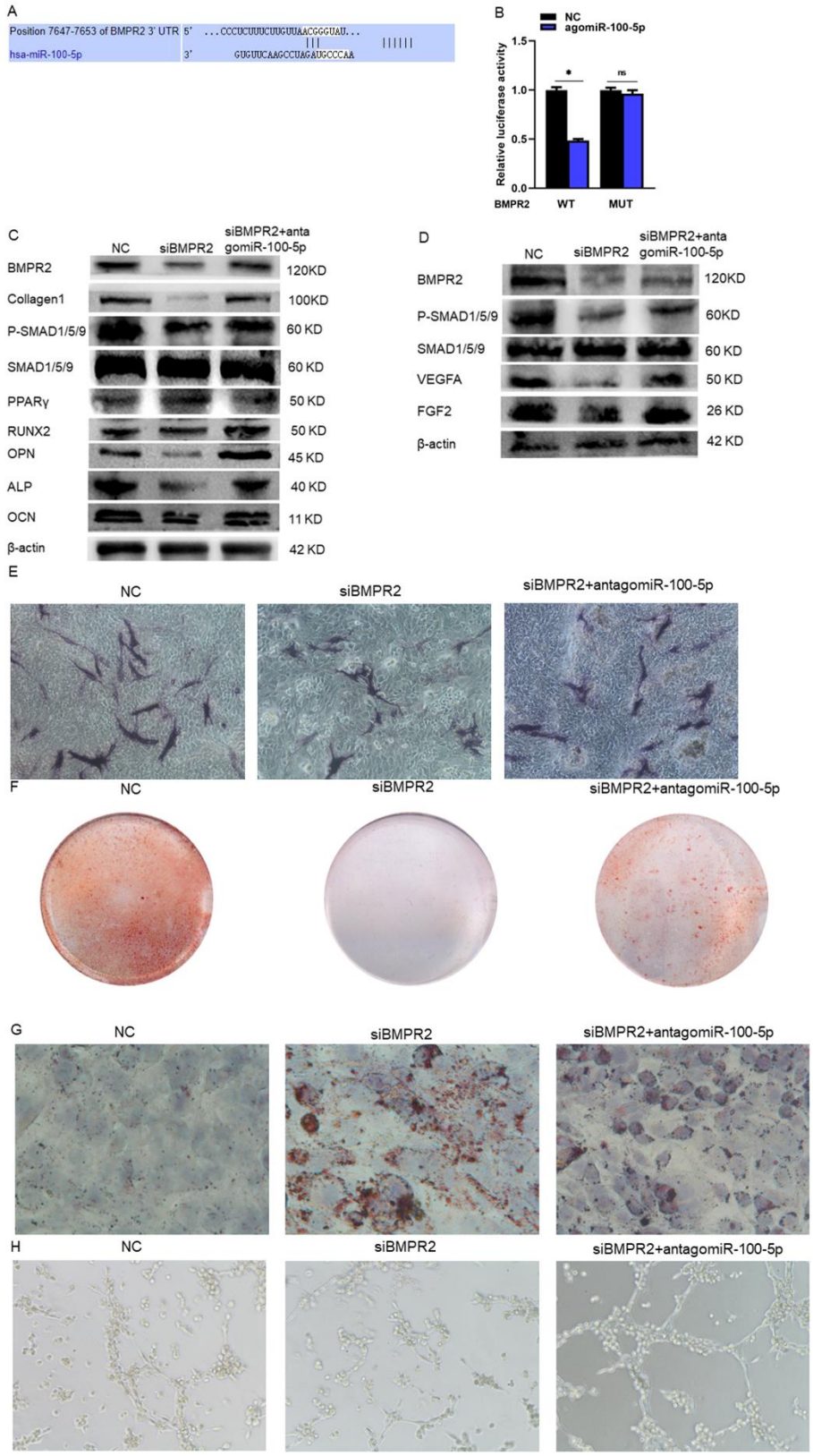

Figure. 7 MiR-100-5p inhibits osteogenesis of BMSCs and angiogenesis of HUVECs by targeting BMPR2 and inhibiting BMPR2/smad1/5/9 pathway. A The target gene of miR-100-5p was predicted using Targetscan 7.2. **B** The targeting relationship between miR-100-5p and BMPR2 was verified by

luciferase assay. **C** The expressions of Collagen1, BMPR2, SMAD1/5/9, p-SMAD1/5/9, OCN, RUNX2, ALP, OPN and PPARγ were measured using WB in BMSCs transfected with NC, siBMPR2 and siBMPR2+antagomiR-100-5p. **D** The expressions of BMPR2, SMAD1/5/9, p-SMAD1/5/9, FGF2 and VEGFA were measured using WB in HUVECs transfected with NC, siBMPR2 and siBMPR2+antagomiR-100-5p. **E** ALP staining of BMSCs. (×100). **F** Alizarin red staining of BMSCs. **G** Oil red staining of BMSCs (×400). **H** Tube formation assay of HUVECs. *P <0.05, versus NC group; #P < 0.05, versus agomiR-100-5p group. All data were expressed as mean ± SEM.

AntagomiR-100-5p rescued the suppression of osteogenesis of BMSCs and angiogenesis of HUVECs caused by NONFH-exosomes

The data of Fig. 7 showed that antagomiR-100-5p remedied the decreased osteogenesis of BMSCs and angiogenesis of HUVECs caused by siBMPR2. Then we further investigated the effect of antagomiR-100-5p on NONFH-exosomes induced NONFH-like impairment model in BMSCs and HUVECs. The results of RT-PCR showed that the expressions of miR-100-5p in BMSCs and HUVECs were down-regulated by antagomir-100-5p (Fig. 8 A, C). To assess the effects of antagomiR-100-5p on osteogenesis of BMSCs treated with NONFH-exosomes, the osteogenic markers was measured by western blotting (Fig. 8 B). The NONFH-induced down-regulation of Collagen1,OCN, ALP, OPN, Runx2, BMPR2 and p-SMAD1/5/9 was dramatically decreased could be partly rescued by the treatment of antagomiR-100-5p The results suggested that antagomiR-100-5p could partly restore the impaired osteogenesis in BMSCs caused by NONFH-exosomes. In addition, the ALP staining and alizarin red S staining demonstrated the similar effect of antagomiR-100-5p on ALP activity and mineralization capacity (Fig. 8 E, F). But the expression of PPARγ and the formatted lipid droplets were increased in BMSCs after treated with NONFH-exosomes, while antagomiR-100-5p could partly suppressed the up-regulation of PPARγ and formatted lipid droplets of BMSCs caused by NONFH-exosomes (Fig.8 B, G). In addition, the western blotting showed transfected with antagomiR-100-5p could partly rescued the down-regulations of FGF2, VEGFA, BMPR2 and p-SMAD1/5/9 of HUVECs caused by NONFH-exosomes (Fig. 8 D). The tube formation assay showed the same trend (Fig. 8 H). These data demonstrated that antagomiR-100-5p were able to restore the influence of NONFH-exosomes on the differentiation of BMSCs and HUVECs.

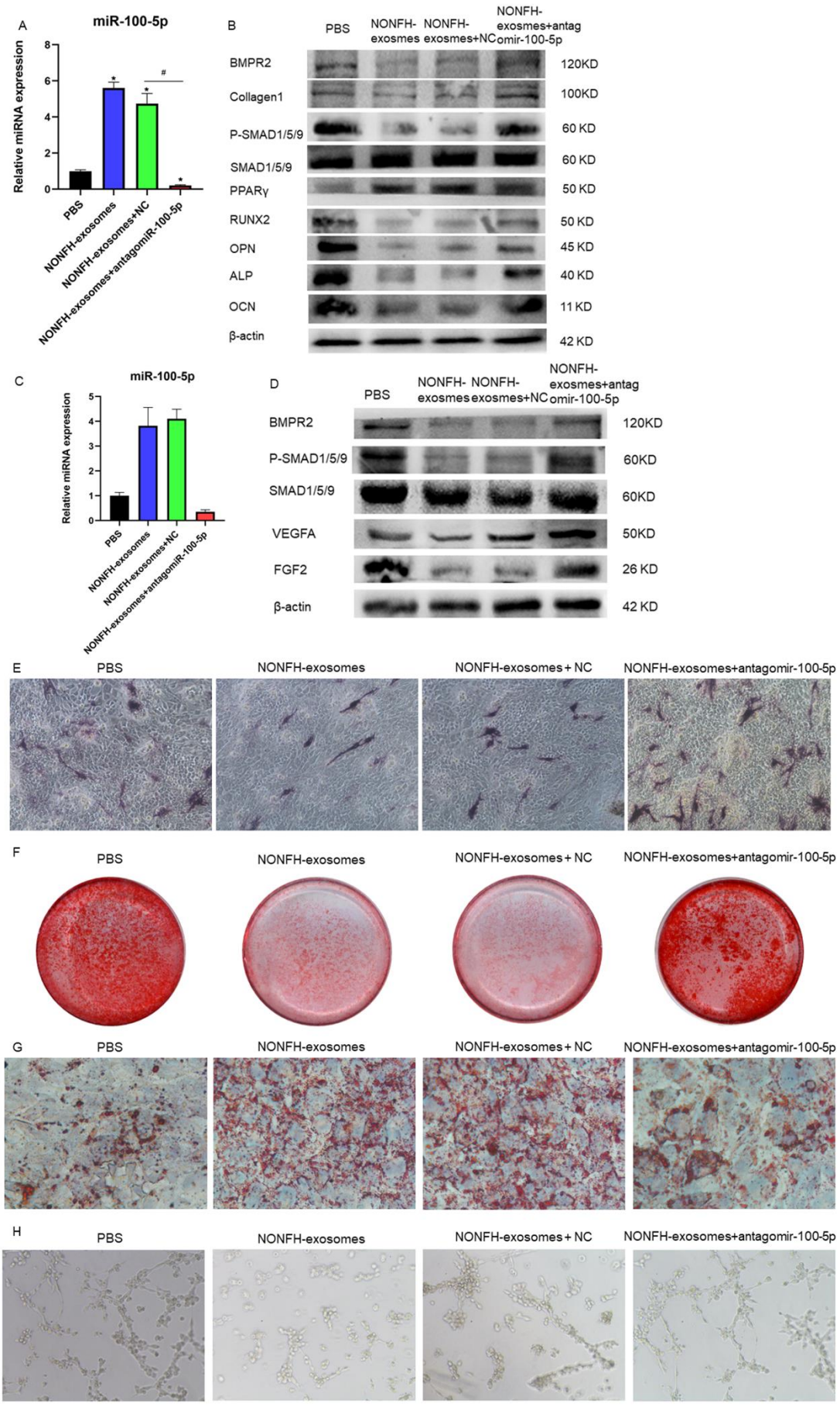
A
miR-100-5p
Relative miRNA expression
PBS
NONFH-exosomes
NONFH-exosomes+NC
NONFH-exosomes+antagomiR-100-5p
B
PBS
NONFH-exosmes
NONFH-exosmes+NC
NONFH-exosmes+antagomir-100-5p
BMPR2
Collagen1
P-SMAD1/5/9
SMAD1/5/9
PPARγ
RUNX2
OPN
ALP
OCN
β-actin
120KD
100KD
60 KD
60 KD
50 KD
50 KD
45 KD
40 KD
11 KD
42 KD
C
miR-100-5p
Relative miRNA expression
PBS
NONFH-exosomes
NONFH-exosomes+NC
NONFH-exosomes+antagomiR-100-5p
D
PBS
NONFH-exosmes
NONFH-exosmes+NC
NONFH-exosmes+antagomir-100-5p
BMPR2
P-SMAD1/5/9
SMAD1/5/9
VEGFA
FGF2
β-actin
120KD
60KD
60KD
50KD
26 KD
42 KD
E
PBS
NONFH-exosomes
NONFH-exosomes+NC
NONFH-exosomes+antagomir-100-5p
F
PBS
NONFH-exosomes
NONFH-exosomes+NC
NONFH-exosomes+antagomir-100-5p
G
PBS
NONFH-exosomes
NONFH-exosomes+NC
NONFH-exosomes+antagomir-100-5p
H
PBS
NONFH-exosomes
NONFH-exosomes+NC
NONFH-exosomes+antagomir-100-5p

Figure.8 AntagomiR-100-5p rescued the suppression of osteogenesis of BMSCs and angiogenesis of HUVECs caused by NONFH-exosomes. A The expressions of miR-100-5p in BMSCs treated with PBS, NONFH-exosomes, NONFH-exosomes + NC and NONFH-exosomes + antagomir-100-5p. **B** The expressions of BMPR2, SMAD1/5/9, p-SMAD1/5/9, Collagen1, OCN, RUNX2, ALP, OPN and PPARγ were measured using WB in BMSCs. **C** The expressions of miR-100-5p in HUVECs treated with PBS, NONFH-exosomes, NONFH-exosomes + NC and NONFH-exosomes + antagomir-100-5p. **D** The expressions of BMPR2, BMPR2, SMAD1/5/9, p-SMAD1/5/9, FGF2 and VEGFA were measured using WB in HUVECs. **E** ALP staining of BMSCs (×100). **F** Alizarin red staining of BMSCs after cultured in ODM for 14 days. **G** Oil red staining of BMSCs (×400). **H** Tube formation assay of HUVECs. *P <0.05, versus NC group; #P < 0.05, versus agomiR-100-5p group. All data were expressed as mean ± SEM.

Discussion

As one of the most common and intractable orthopedic diseases, NONFH eventually leads to physical and mental handicap in young adults[37-39]. For the difficulty in early diagnosis and its irreversible progress, NONFH result in heavy economic burden[40]. Based on previous studies, the pathogenesis of NONFH can be mainly summarized as follows :(I) impaired angiogenesis of vascular endothelial cells and (II) reduced osteogenic activity and increased adipogenesis of BMSCs[41-44]. In this study, we found that expressions of osteogenic and angiogenic markers were decreased in necrotic bone tissue of NONFH, accompanied with an augment of adipogenic marker.

Exosomes derived from different mesenchymal stem cells has been reported to be a popular area of research for the treatment of NONFH[9, 25, 27]. The most popular therapeutic mechanisms of multiple MSC-derived exosomes were promoting osteogenic differentiation BMSCs and angiogenic differentiation of VECs. However, there was no study that thoroughly explored the role of exosomes in the pathogenesis of NONFH. In addition, the research of multi-source exosomes isolated from the bone microenvironment might be more proper for disclosing the signals released from the necrotic tissues in NONFH. In this study, our results showed that NONFH-exosomes were able to induce NONFH-like damage on BMSCs, HUVECs, and S-D rats. As the dysfunction of osteogenesis of BMSCs and angiogenesis of vascular endothelial cells (VECs) were key processes during NONFH, it was inferred that NONFH-exosomes might cause NONFH by suppressing osteogenesis of BMSCs and angiogenesis of vascular endothelial cells.

Among the studies before, the expression of miR-100-5p was up-regulated in the blood serum of NONFH patients. In our study, we found that miR-100-5p was up-regulated in NONFH-exosomes and the up-regulation of exosomal miR-100-5p could inhibited angiogenesis of HUVECs and osteogenesis of BMSCs, promoting adipogenesis of BMSCs.

BMPR2, an important role in BMP-SMAD signaling, was reported to be down-regulated in blood serum. In this study, we found that the expression of BMPR2 was inhibited by NONFH-exosomes and miR-100-5p, leading to the suppression of p-

SMAD1/5/9 and the inactivation of BMP-SMAD signaling. This finally result in the reduction of osteogenesis of BMSCs and angiogenesis of HUVECs with the augment of adipogenesis of BMSCs.

Conclusion

In conclusion, our study demonstrated that NONFH-exosomal miR-100-5p facilitated NONFH through suppressing differentiation of BMSCs and VECs by targeting BMPR2 and inactivating BMPR2/Smad1/5/9 signaling pathway. Our study also showed that the inhibition of miR-100-5p could rescue the NONFH-like damage in BMSCs and HUVECs caused by NONFH-exosomes by activating BMPR2/Smad1/5/9 signaling pathway. This study would also provide us with clues for thoroughly exploring the pathomechanism and identifying potential solutions for NONFH and the failure of cell therapy.

Data Availability Statement

All data generated or analyzed during this study are included in this article.

List of Abbreviations

qRT-PCR Quantitative real-time polymerase chain reaction
ALP Alkaline phosphatase
ARS Alizarin Red S
BCA Bicinchoninic acid
BMI Body mass index
BMPR2 Bone Morphogenetic Protein receptor 2
BMSCs bone marrow mesenchymal stem cells
BSA Bovine serum albumin
BV/TV Bone volume per tissue volume
DLS Dynamic light scattering
FBS Fetal bovine serum
FGF2 fibroblast growth factor 2
FNF Femoral neck fracture
HE Hematoxylin and Eeosin
IHC Immunohistochemistry
HUVECs Human Umbilical Vein Endothelial Cells
IHC Immunohistochemistry
KEGG Kyoto Encyclopedia of Genes and Genomes
NC Negative control

NONFH Non-traumatic osteonecrosis of the femoral head
NTA Nanoparticle tracking analysis
OCN Osteocalcin
OPN Osteopontin
PBS Phosphate Buffer Saline

PPARγ Peroxisome proliferator-actiated receptor γ

RUNX2 Runt-related transcription factor 2

SDS-PAGE Sodium dodecyl sulfate polyacrylamide gel electrophoresis
SEM Standard error of mean
Tb.N Trabecular number
Tb.Sp Trabecular separation
Tb.Th Trabecular thickness
TBST Tris-buffered saline/Tween-20 buffer
TEM Transmission electron microscopy
VECs Vascular endothelial cells
VEGFA Vascular Endothelial Growth Factor
3'UTR 3′-Untranslated region

Declarations

Ethics approval and consent to participate

This study was approved by the Research Ethics Committee of The Affiliated Hospital of Chongqing Medical University. Approved by the Institutional Review Committee of the First Affiliated Hospital of Chongqing Medical University, a informed consensus was signed by each donor. All animal studies complied with the principles based on the International Guiding Principles for Biomedical Research Involving Animals.

Consent for publication

Not applicable.

Availability of data and materials

All data used and analyzed during the current study are available from the corresponding author on reasonable request.

Funding

This work was funded by Medical Research Project of Health and Family Planning Commission in Chongqing (Grant No. 2017ZDXM006) and General Project of Technology Innovation and Application Development of Chongqing Science and Technology Bureau (Grant No. cstc2019jscx-msxmX0245).

Authors' contributions

Wu Yang contributed to the most experiments and writing of the original manuscript. Weiwen Zhu and Tingmei Chen contributed to the conceptualization. Yunfei Yang contributed to the data analysis and review. Zijie Xu contributed to the investigation. Husun Qian and Minkang Guo contributed to the animal experiments. Haobo Bai contributed to the radiological examination. Chengjie Lian contributed to discussion. Weiqian Jiang and Yu Chen contributed resources. Jian Zhang was responsible for the project administration and funding acquisition. All authors read and approved the final manuscript.

Competing interests

The authors declare that they have no competing interests.

Acknowledgements

We appreciate the Key Laboratory of Diagnostic Medicine Designated by the Ministry of Education, Chongqing Medical University for providing experimental platform.

Reference

1. Moya-Angeler J, Gianakos AL, Villa JC, Ni A, Lane JM. Current concepts on osteonecrosis

of the femoral head. World J Orthop. 2015 Sep 18;6(8):590-601.
2. Mont MA, Salem HS, Piuzzi NS, Goodman SB, Jones LC. Nontraumatic Osteonecrosis of the Femoral Head: Where Do We Stand Today?: A 5-Year Update. J Bone Joint Surg Am. 2020 Jun 17;102(12):1084-1099.
3. Mont MA, Cherian JJ, Sierra RJ, Jones LC, Lieberman JR. Nontraumatic Osteonecrosis of the Femoral Head: Where Do We Stand Today? A Ten-Year Update. J Bone Joint Surg Am. 2015 Oct 7;97(19):1604-27.
4. Lei P, Du W, Liu H, Wu P, Zhou Z, Yu F, Qing L, Pan D, Liu R, Zeng L, Cao Z, Ou Q, Tang J. Free vascularized iliac bone flap based on deep circumflex iliac vessels graft for the treatment of osteonecrosis of femoral head. J Orthop Surg Res. 2019 Nov 28;14(1):397.
5. Liu F, Wang W, Yang L, Wang B, Wang J, Chai W, Zhao D. An epidemiological study of etiology and clinical characteristics in patients with nontraumatic osteonecrosis of the femoral head. J Res Med Sci. 2017 Feb 16;22:15.
6. Lee YJ, Cui Q, Koo KH. Is There a Role of Pharmacological Treatments in the Prevention or Treatment of Osteonecrosis of the Femoral Head?: A Systematic Review. J Bone Metab. 2019 Feb;26(1):13-18. doi: 10.11005/jbm.2019.26.1.13. Epub 2019 Feb 28.
7. Zhu W, Guo M, Yang W, Tang M, Chen T, Gan D, Zhang D, Ding X, Zhao A, Zhao P, Yan W, Zhang J. CD41-deficient exosomes from non-traumatic femoral head necrosis tissues impair osteogenic differentiation and migration of mesenchymal stem cells. Cell Death Dis. 2020 Apr 27;11(4):293.
8. Wu F, Jiao J, Liu F, Yang Y, Zhang S, Fang Z, Dai Z, Sun Z. Hypermethylation of Frizzled1 is associated with Wnt/β-catenin signaling inactivation in mesenchymal stem cells of patients with steroid-associated osteonecrosis. Exp Mol Med. 2019 Feb 26;51(2):1-9.
9. Zuo R, Kong L, Wang M, Wang W, Xu J, Chai Y, Guan J, Kang Q. Exosomes derived from human CD34+ stem cells transfected with miR-26a prevent glucocorticoid-induced osteonecrosis of the femoral head by promoting angiogenesis and osteogenesis. Stem Cell Res Ther. 2019 Nov 15;10(1):321.
10. Bianco P. "Mesenchymal" stem cells. Annu Rev Cell Dev Biol. 2014;30:677-704.
11. Wang B-L, Sun W, Shi Z-C, et al. Decreased proliferation of mesenchymal stem cells in corticosteroid-induced osteonecrosis of femoral head. Orthopedics. 2008;31(5):444.
12. Kerachian MA, Harvey EJ, Cournoyer D, Chow TY, Séguin C. Avascular necrosis of the femoral head: vascular hypotheses. Endothelium. 2006 Jul-Aug;13(4):237-44.
13. Aschbacher K, Derakhshandeh R, Flores AJ, Narayan S, Mendes WB, Springer ML. Circulating angiogenic cell function is inhibited by cortisol in vitro and associated with psychological stress and cortisol in vivo. Psychoneuroendocrinology. 2016 May;67:216-23.
14. Stefanius K, Servage K, de Souza Santos M, Gray HF, Toombs JE, Chimalapati S, Kim MS, Malladi VS, Brekken R, Orth K. Human pancreatic cancer cell exosomes, but not human normal cell exosomes, act as an initiator in cell transformation. Elife. 2019 May 28;8:e40226.
15. Li D, Liu J, Guo B, Liang C, Dang L, Lu C, He X, Cheung HY, Xu L, Lu C, He B, Liu B, Shaikh AB, Li F, Wang L, Yang Z, Au DW, Peng S, Zhang Z, Zhang BT, Pan X, Qian A, Shang P, Xiao L, Jiang B, Wong CK, Xu J, Bian Z, Liang Z, Guo DA, Zhu H, Tan W, Lu A, Zhang G. Osteoclast-derived exosomal miR-214-3p inhibits osteoblastic bone formation. Nat Commun. 2016 Mar 7;7:10872.
16. Luo P, Jiang C, Ji P, Wang M, Xu J. Exosomes of stem cells from human exfoliated

deciduous teeth as an anti-inflammatory agent in temporomandibular joint chondrocytes via miR-100-5p/mTOR. Stem Cell Res Ther. 2019 Jul 29;10(1):216.
17.Song H, Li X, Zhao Z, Qian J, Wang Y, Cui J, Weng W, Cao L, Chen X, Hu Y, Su J. Reversal of Osteoporotic Activity by Endothelial Cell-Secreted Bone Targeting and Biocompatible Exosomes. Nano Lett. 2019 May 8;19(5):3040-3048.
18. Wang Z, Yan K, Ge G, Zhang D, Bai J, Guo X, Zhou J, Xu T, Xu M, Long X, Hao Y, Geng D. Exosomes derived from miR-155-5p-overexpressing synovial mesenchymal stem cells prevent osteoarthritis via enhancing proliferation and migration, attenuating apoptosis, and modulating extracellular matrix secretion in chondrocytes. Cell Biol Toxicol. 2020 Oct 25.
19. Zhang L, Jiao G, Ren S, Zhang X, Li C, Wu W, Wang H, Liu H, Zhou H, Chen Y. Exosomes from bone marrow mesenchymal stem cells enhance fracture healing through the promotion of osteogenesis and angiogenesis in a rat model of nonunion. Stem Cell Res Ther. 2020 Jan 28;11(1):38.
20. Cui Y, Luan J, Li H, Zhou X, Han J. Exosomes derived from mineralizing osteoblasts promote ST2 cell osteogenic differentiation by alteration of microRNA expression. FEBS Lett. 2016 Jan;590(1):185-92.
21. Li D, Liu J, Guo B, Liang C, Dang L, Lu C, He X, Cheung HY, Xu L, Lu C, He B, Liu B, Shaikh AB, Li F, Wang L, Yang Z, Au DW, Peng S, Zhang Z, Zhang BT, Pan X, Qian A, Shang P, Xiao L, Jiang B, Wong CK, Xu J, Bian Z, Liang Z, Guo DA, Zhu H, Tan W, Lu A, Zhang G. Osteoclast-derived exosomal miR-214-3p inhibits osteoblastic bone formation. Nat Commun. 2016 Mar 7;7:10872.
22.Ekström K, Omar O, Granéli C, Wang X, Vazirisani F, Thomsen P. Monocyte exosomes stimulate the osteogenic gene expression of mesenchymal stem cells. PLoS One. 2013 Sep 18;8(9):e75227. doi: 10.1371/journal.pone.0075227.
23. Furuta T, Miyaki S, Ishitobi H, Ogura T, Kato Y, Kamei N, Miyado K, Higashi Y, Ochi M. Mesenchymal Stem Cell-Derived Exosomes Promote Fracture Healing in a Mouse Model. Stem Cells Transl Med. 2016 Dec;5(12):1620-1630.
24. Li L, Wang Y, Yu X, Bao Y, An L, Wei X, Yu W, Liu B, Li J, Yang J, Xia Y, Liu G, Cao F, Zhang X, Zhao D. Bone marrow mesenchymal stem cell-derived exosomes promote plasminogen activator inhibitor 1 expression in vascular cells in the local microenvironment during rabbit osteonecrosis of the femoral head. Stem Cell Res Ther. 2020 Nov 11;11(1):480.
25. Tao SC, Yuan T, Rui BY, Zhu ZZ, Guo SC, Zhang CQ. Exosomes derived from human platelet-rich plasma prevent apoptosis induced by glucocorticoid-associated endoplasmic reticulum stress in rat osteonecrosis of the femoral head via the Akt/Bad/Bcl-2 signal pathway. Theranostics. 2017 Jan 15;7(3):733-750.
26. Guo SC, Tao SC, Yin WJ, Qi X, Sheng JG, Zhang CQ. Exosomes from Human Synovial-Derived Mesenchymal Stem Cells Prevent Glucocorticoid-Induced Osteonecrosis of the Femoral Head in the Rat. Int J Biol Sci. 2016 Oct 17;12(10):1262-1272.
27. Kuang MJ, Huang Y, Zhao XG, Zhang R, Ma JX, Wang DC, Ma XL. Exosomes derived from Wharton's jelly of human umbilical cord mesenchymal stem cells reduce osteocyte apoptosis in glucocorticoid-induced osteonecrosis of the femoral head in rats via the miR-21-PTEN-AKT signalling pathway. Int J Biol Sci. 2019 Jul 20;15(9):1861-1871.

28. Fabian MR, Sonenberg N, Filipowicz W. Regulation of mRNA translation and stability by microRNAs. Annu Rev Biochem. 2010;79:351–379.
29. Guo H, Ingolia NT, Weissman JS, Bartel DP. Mammalian microRNAs predominantly act to decrease target mRNA levels. Nature. 2010;466:835–840.
30.Lau NC, Lim LP, Weinstein EG, Bartel DP. An abundant class of tiny RNAs with probable regulatory roles in Caenorhabditis elegans. Science. 2001;294:858–862.
31. Lagos-Quintana M, Rauhut R, Lendeckel W, Tuschl T. Identification of novel genes coding for small expressed RNAs. Science. 2001;294:853–858.
32. Kong L, Zuo R, Wang M, Wang W, Xu J, Chai Y, Guan J, Kang Q. Silencing MicroRNA-137-3p, which Targets RUNX2 and CXCL12 Prevents Steroid-induced Osteonecrosis of the Femoral Head by Facilitating Osteogenesis and Angiogenesis. Int J Biol Sci. 2020 Jan 14;16(4):655-670.
33. Peng Q, Zhang L, Li J, Wang W, Cai J, Ban Y, Zhou Y, Hu M, Mei Y, Zeng Z, Li X, Xiong W, Li G, Tan Y, Xiang B, Yi M. FOXA1 Suppresses the Growth, Migration, and Invasion of Nasopharyngeal Carcinoma Cells through Repressing miR-100-5p and miR-125b-5p. J Cancer. 2020 Feb 10;11(9):2485-2495.
34. Ye Y, Li SL, Wang JJ. miR-100-5p Downregulates mTOR to Suppress the Proliferation, Migration, and Invasion of Prostate Cancer Cells. Front Oncol. 2020 Dec 1;10:578948.
35. Li D, Yu K, Xiao T, Dai Y, Liu L, Li H, Jiang D, Xiong L. LOC103691336/miR-138-5p/BMPR2 axis modulates Mg-mediated osteogenic differentiation in rat femoral fracture model and rat primary bone marrow stromal cells. J Cell Physiol. 2019 Nov;234(11):21316-21330.
36. Finkenzeller G, Hager S, Stark GB. Effects of bone morphogenetic protein 2 on human umbilical vein endothelial cells. Microvasc Res. 2012 Jul;84(1):81-5.
37. Zhuang L, Wang L, Xu D, Wang Z. Anteromedial femoral neck plate with cannulated screws for the treatment of irreducible displaced femoral neck fracture in young patients: a preliminary study. Eur J Trauma Emerg Surg. 2019 Dec;45(6):995-1002.
38. Wang C, Sun W, Ling S, et al. AAV-Anti-miR-214 prevents collapse of the femoral head in osteonecrosis by regulating osteoblast and osteoclast activities. Mol Ther Nucleic Acids. 2019;18:841-850.
39. Rocchi M, Del Piccolo N, Mazzotta A, Giavaresi G, Fini M, Facchini F, Stagni C, Dallari D. Core decompression with bone chips allograft in combination with fibrin platelet-rich plasma and concentrated autologous mesenchymal stromal cells, isolated from bone marrow: results for the treatment of avascular necrosis of the femoral head after 2 years minimum follow-up. Hip Int. 2020 Dec;30(2_suppl):3-12.
40.Yang F, Wei Q, Chen X, Hong G, Chen Z, Chen Y, He W. Vascularized pedicle iliac bone grafts as a hip-preserving surgery for femur head necrosis: a systematic review. J Orthop Surg Res. 2019 Aug 27;14(1):270.
41. Zhang C, Su Y, Ding H, Yin J, Zhu Z, Song W. Mesenchymal stem cells-derived and siRNAs-encapsulated exosomes inhibit osteonecrosis of the femoral head. J Cell Mol Med. 2020 Sep;24(17):9605-9612.
42.Yao X, Yu S, Jing X, Guo J, Sun K, Guo F, Ye Y. PTEN inhibitor VO-OHpic attenuates GC-associated endothelial progenitor cell dysfunction and osteonecrosis of the femoral head via activating Nrf2 signaling and inhibiting mitochondrial apoptosis pathway. Stem Cell Res

Ther. 2020 Mar 30;11(1):140.
43.Yu H, Zhu D, Liu P, Yang Q, Gao J, Huang Y, Chen Y, Gao Y, Zhang C. Osthole stimulates bone formation, drives vascularization and retards adipogenesis to alleviate alcohol-induced osteonecrosis of the femoral head. J Cell Mol Med. 2020 Apr;24(8):4439-4451.
44.Yu H, Liu P, Zhu D, Yin J, Yang Q, Huang Y, Chen Y, Zhang C, Gao Y. Chrysophanic acid shifts the differentiation tendency of BMSCs to prevent alcohol-induced osteonecrosis of the femoral head. Cell Prolif. 2020 Aug;53(8):e12871.
45. Wei B, Wei W, Wang L, Zhao B. Differentially Expressed MicroRNAs in Conservatively Treated Nontraumatic Osteonecrosis Compared with Healthy Controls. Biomed Res Int. 2018 May 24;2018:9015758.
46. Yeh CS, Chung FY, Chen CJ, Tsai WJ, Liu HW, Wang GJ, Lin SR. PPARgamma-2 and BMPR2 genes were differentially expressed in peripheral blood of SLE patients with osteonecrosis. DNA Cell Biol. 2008 Nov;27(11):623-8.

Figures

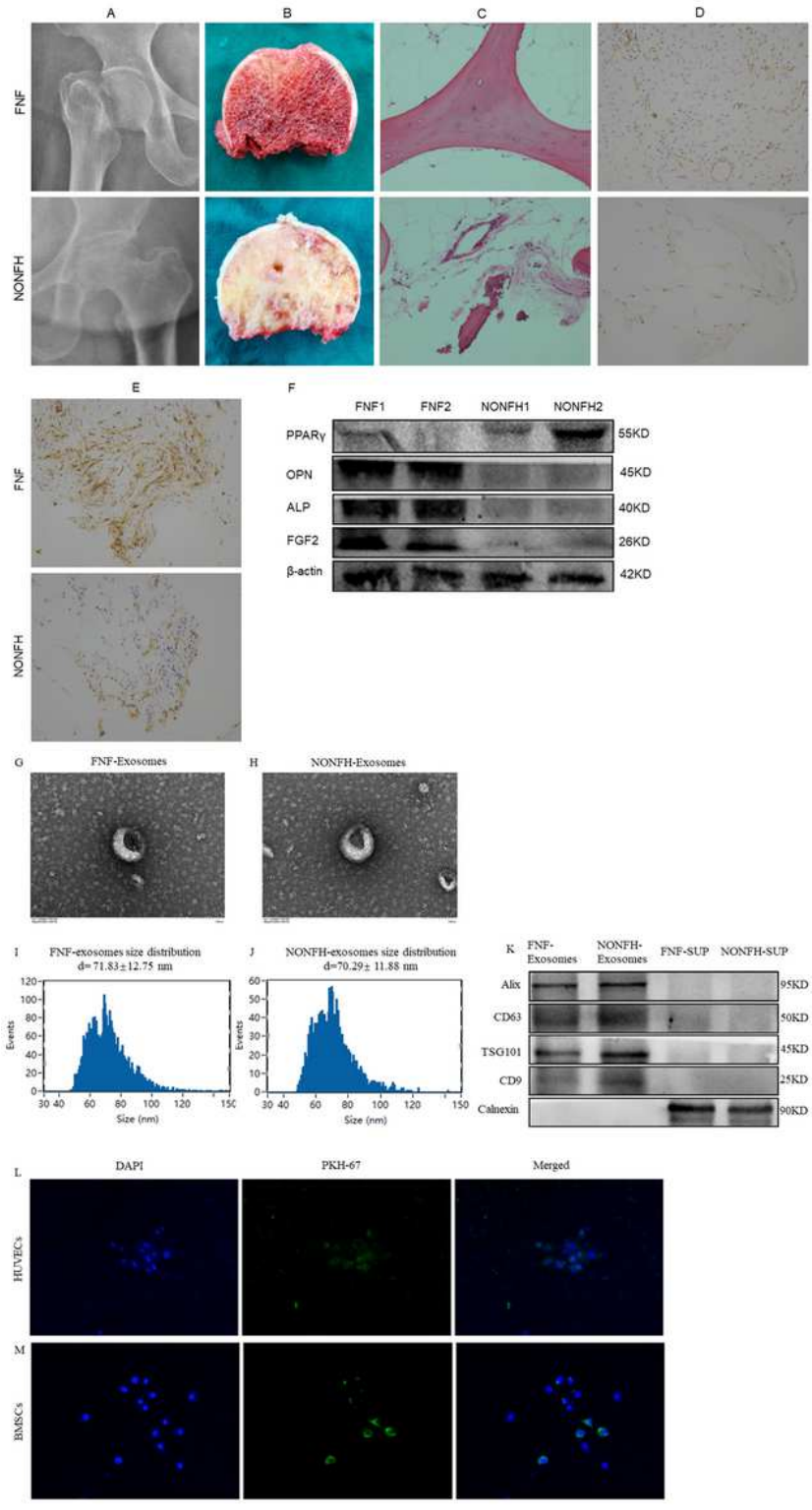

Figure 1

Characteristics of NONFH samples, FNF samples, NONFH-exosomes and FNF-exosomes. A-C Representative X-rays (A), sectional images (B), and HE stainings (C) of femoral heads from FNF and NONFH patients (××100). D-E IHC stainings of CD31 (D) and RUNX2 (E) were conducted in femoral heads

of FNF and NONFH patients (×200). F The expressions of PPARγγ, OPN, ALP, FGF2 were measured by western blotting. G-H TEM images displayed the double membrane and discoid shape of FNF-exosomes (G) and NONFH-exosomes (H) (scale bar=100 nm). I-J Particle size distributions of FNF-exosomes (I) and NONFH-exosomes (J) were measured by NTA. K The expressions of CD63, CD9, Alix, Calnexin and TSG101 in FNF-exosomes, NONFH-exosomes, and the FNF-supernatants (FNF-SUP) and NONFH-supernatants (NONFH-SUP) were examined by western blotting. F, G Observation of PKH-67-labeled exosomes were uptaken into BMSCs and HUVECs under the fluorescence microscopy (×200, scale bar=50 μm), where green (PKH-67) indicates exosomes and blue (DAPI) indicates BMSCs and HUVECs.

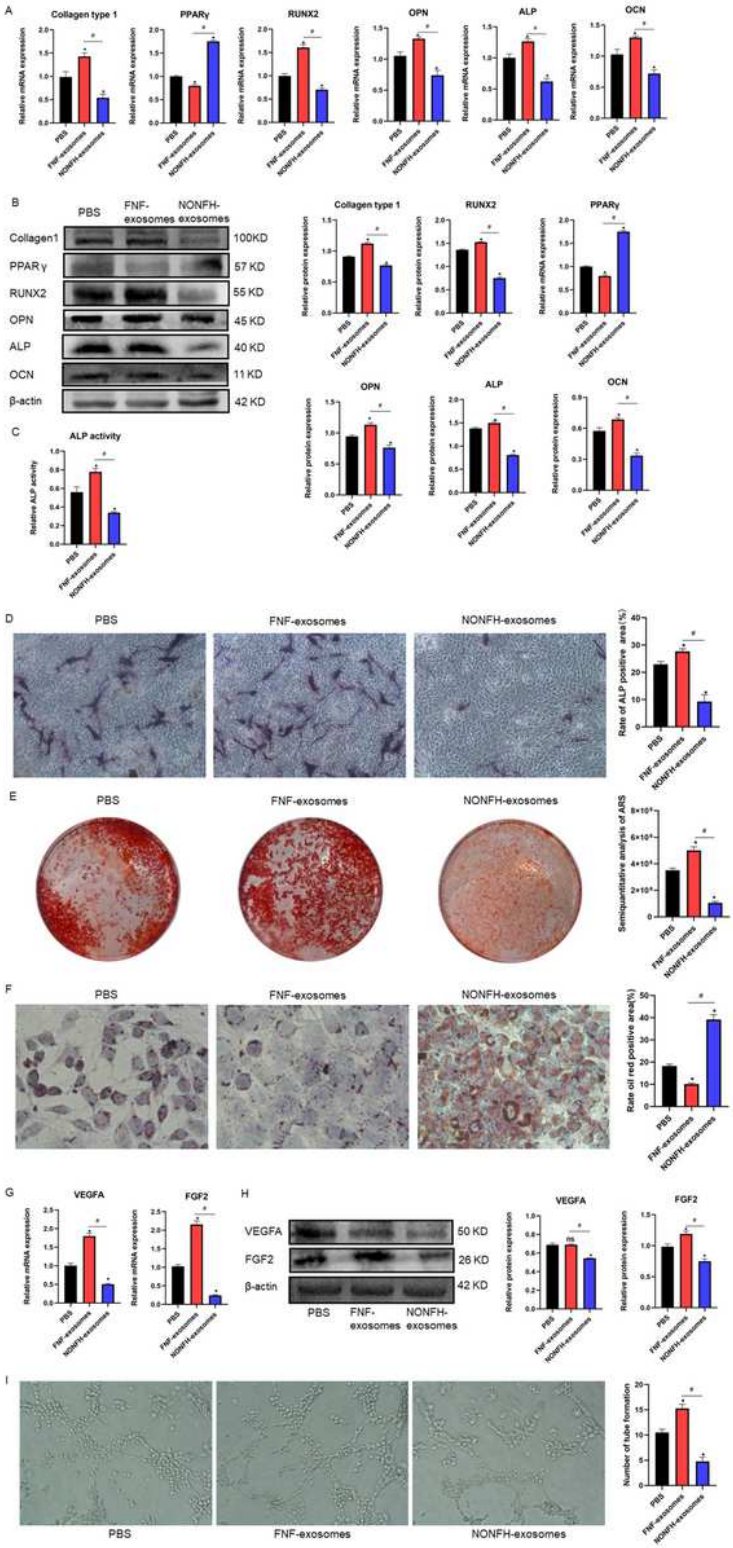

Figure 2

NONFH-exosomes inhibited osteogenic differentiation and promoted adipogenic differentiation of BMSCs. A-B The expressions of Collagen1, OCN, RUNX2, ALP, OPN and PPARγ were measured by RT-PCR (A) and WB (B) in BMSCs treated with PBS, FNF-exosomes, or NONFH-exosomes. C-D ALP activity and ALP staining of BMSCs . (×100). E Alizarin red staining of BMSCs. F Oil red staining of BMSCs (×400). G-H The expressions of VEGFA, FGF2 were measured by RT-PCR (G) and western blotting (H). I Tube

formation assay of HUVECsl. *P <0.05, versus PBS group; #P < 0.05, versus FNF-exosomes group. All data were expressed as mean ± SEM.

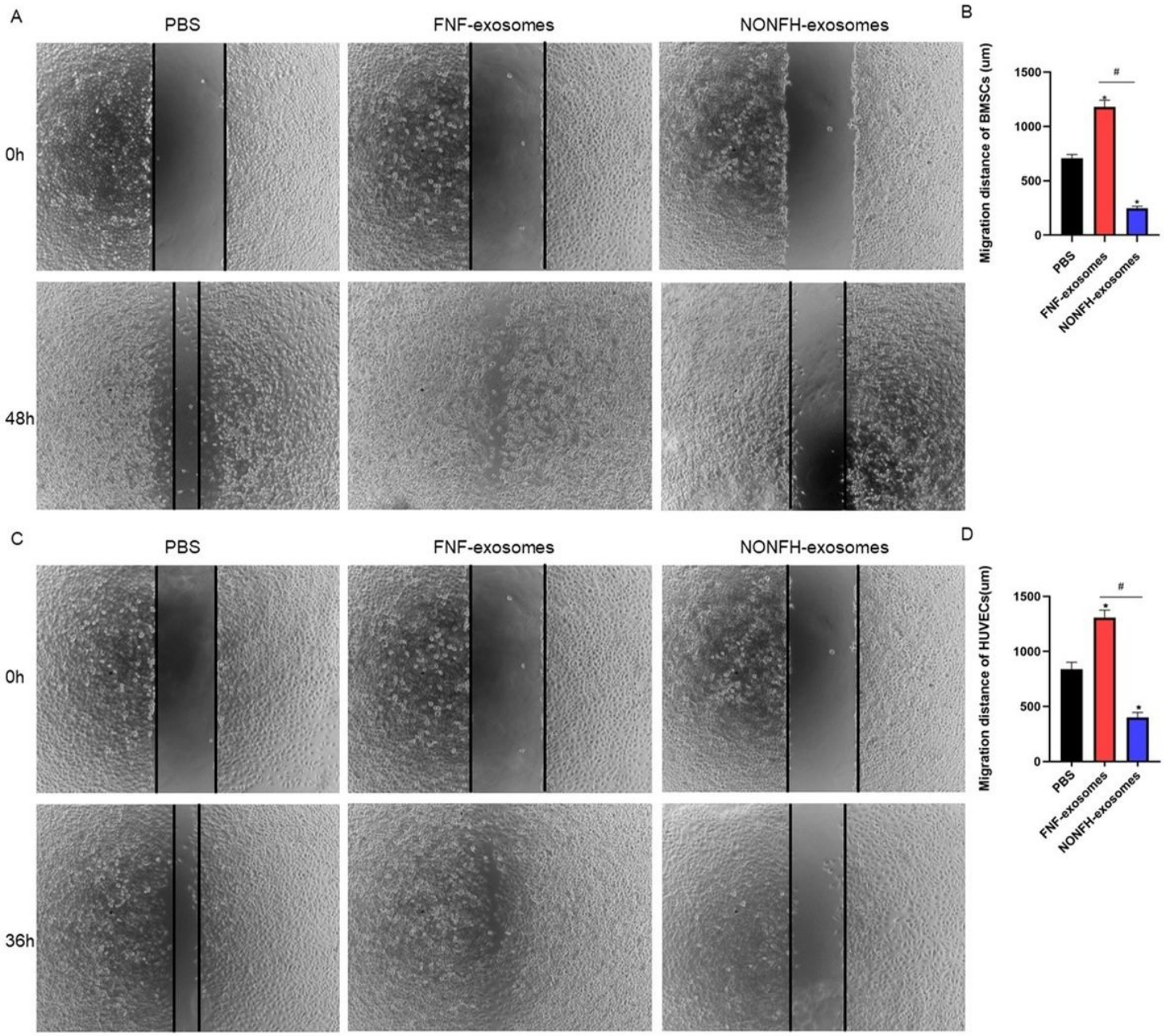

Figure 3

NONFH-exosomes inhibited the migration ability of BMSCs and HUVECs. A-B Wound healing assay of BMSCs (A) and its quantitative analysis (B). C-D Wound healing assay of HUVECs (C) and its quantitative analysis (D). *P <0.05, versus PBS group; #P < 0.05, versus FNF-exosomes group. All data were expressed as mean ± SEM.

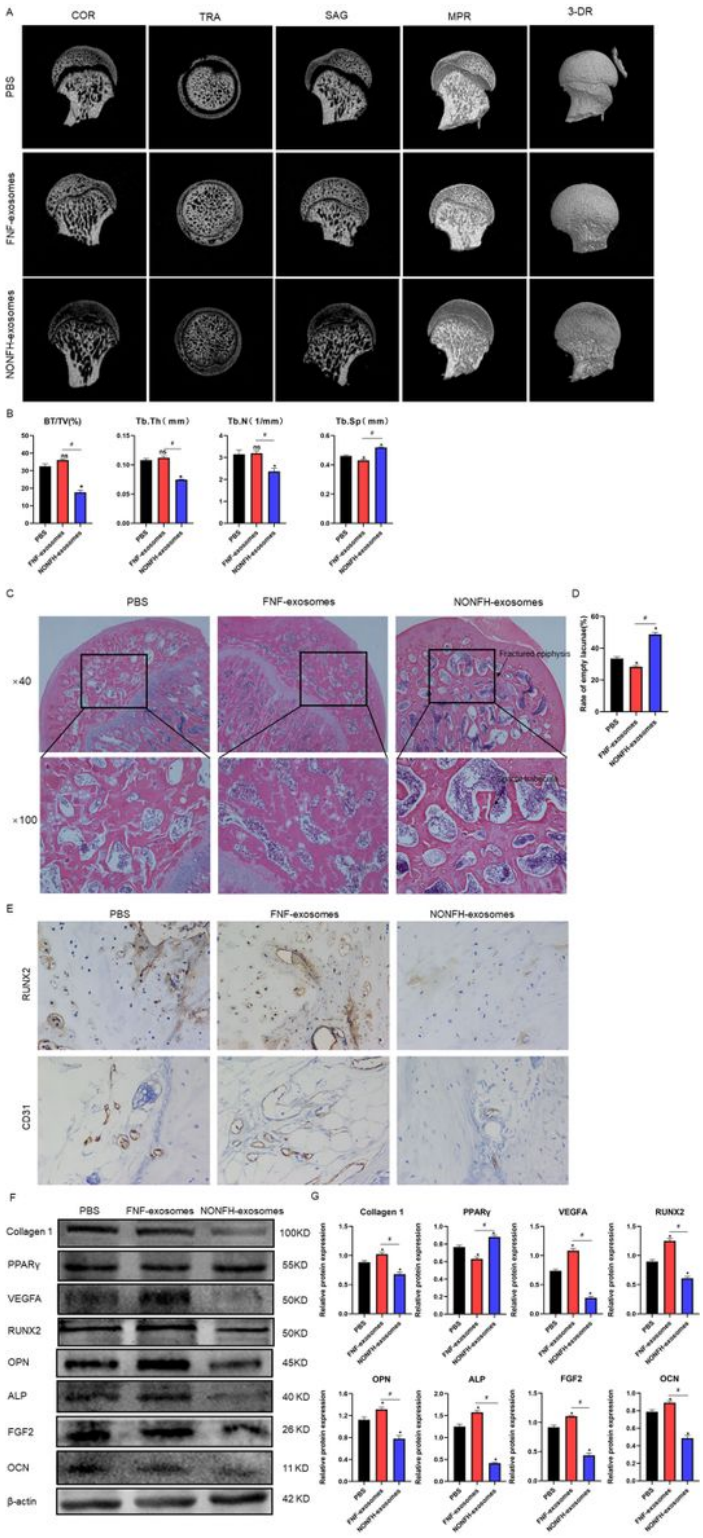

Figure 4

NONFH-exosomes could lead to NONFH-like damage on rats. A COR, TRA, SAG, MPR, and 3-DR images of rat femoral heads. COR, coronal; TRA, transverse; SAG, sagittal; MPR, multiplanar reconstruction; 3-DR, three-dimensional reconstruction. B Quantitative analysis of micro-CT scanning. BV/TV, bone volume per tissue volume; Tb.N, trabecular number; Tb.Sp, trabecular separation; Tb.Th, Trabecular thickness. C HE stainings of the femoral heads. D Quantitative analysis of marrow cavity. E The expression of RUNX2,

CD31 in the femoral head of rats were measured by IHC staining(P < 0.05). F Western blot was used to detect the expression of Collagen1, VEGFA, FGF2, RUNX2, OPN, PPARγ, ALP, and OCN in femoral heads of rats. G Quantitative analysis of WB. *P <0.05, versus PBS group; #P < 0.05, versus FNF-exosomes group. All data were expressed as mean ± SEM.

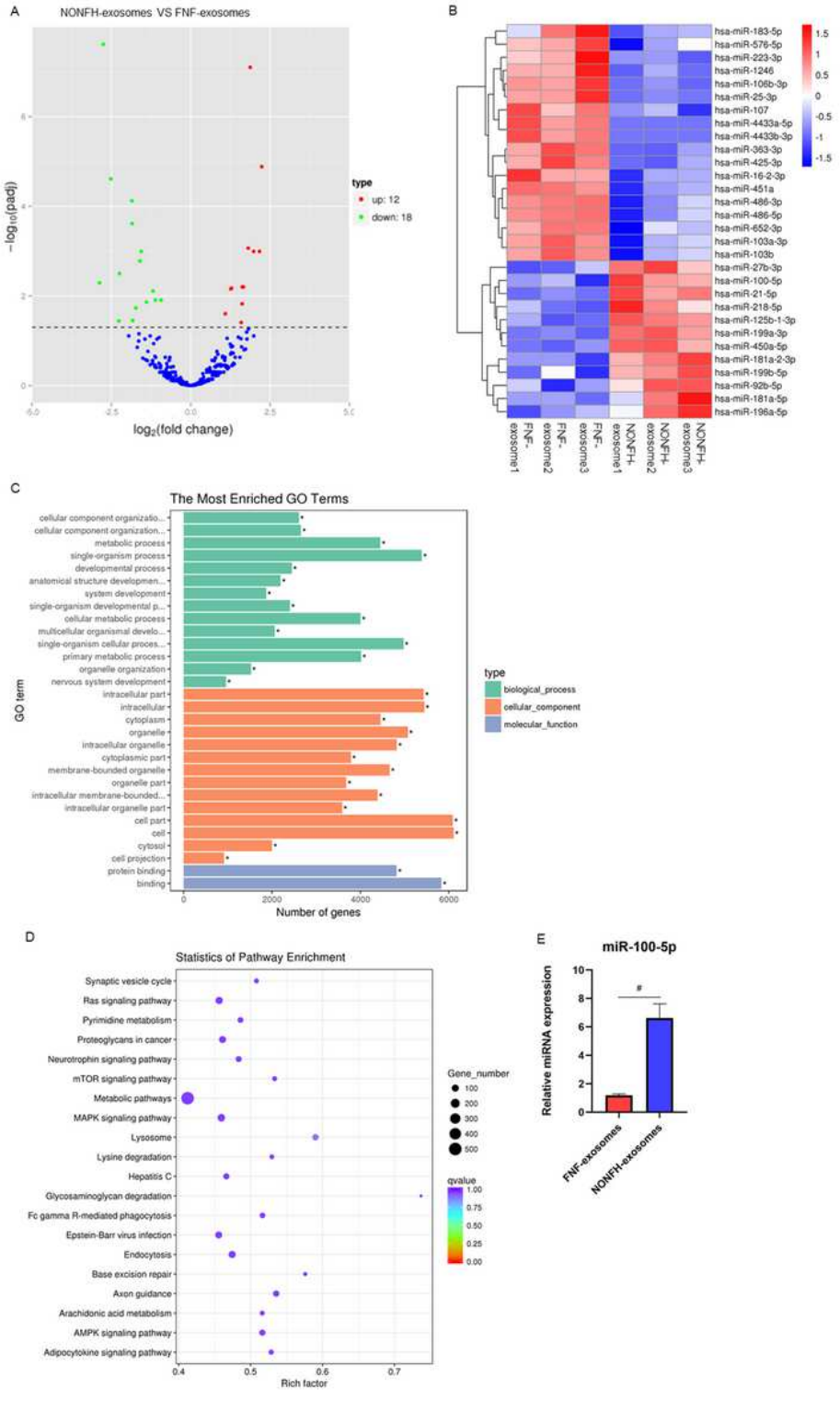

Figure 5

MiR-100-5p was up-regulated in NONFH-exosomes. A Volcano map of the miRNA sequencing. B Heatmap of the miRNA sequencing (B). C GO enrichment. D KEGG pathway enrichment. E RT-PCR was used to detect the expression of miR-100-5p in FNF-exosomes and NONFH-exosomes. #P < 0.05, versus FNF-exosomes group. All data were expressed as mean ± SEM.

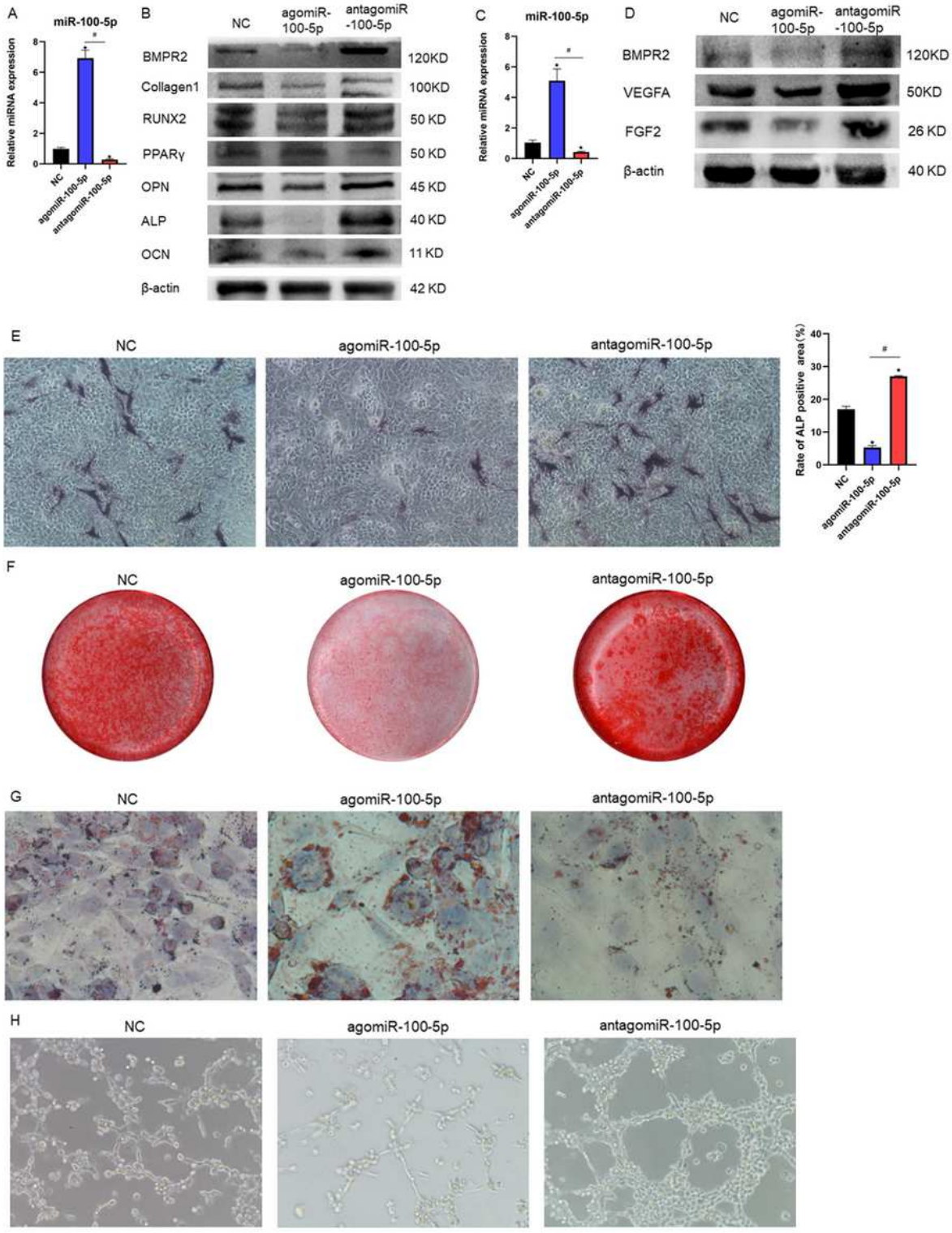

Figure 6

MiR-100-5p inhibited osteogenesis of BMSCs and angiogenesis of HUVECs, promoting adipogenesis of BMSCs. A The expressions of miR-100-5p in BMSCs transfected with NC, agomiR-100-5p and antagomir-100-5p.B The expressions of BMPR2, Collagen1, OCN, RUNX2, ALP, OPN and PPARγ were measured using WB in BMSCs. C The expressions of miR-100-5p in HUVECs transfected with NC, agomiR-100-5p and antagomir-100-5p. D The expressions of BMPR2, FGF2 and VEGFA were measured using WB in HUVECs. E ALP staining of BMSCs. (×100). F Alizarin red staining of BMSCs after cultured in ODM for 14 days. G Oil red staining of BMSCs (×400). H Tube formation assay of HUVECs. *P <0.05, versus NC group; #P < 0.05, versus agomiR-100-5p group. All data were expressed as mean ± SEM.

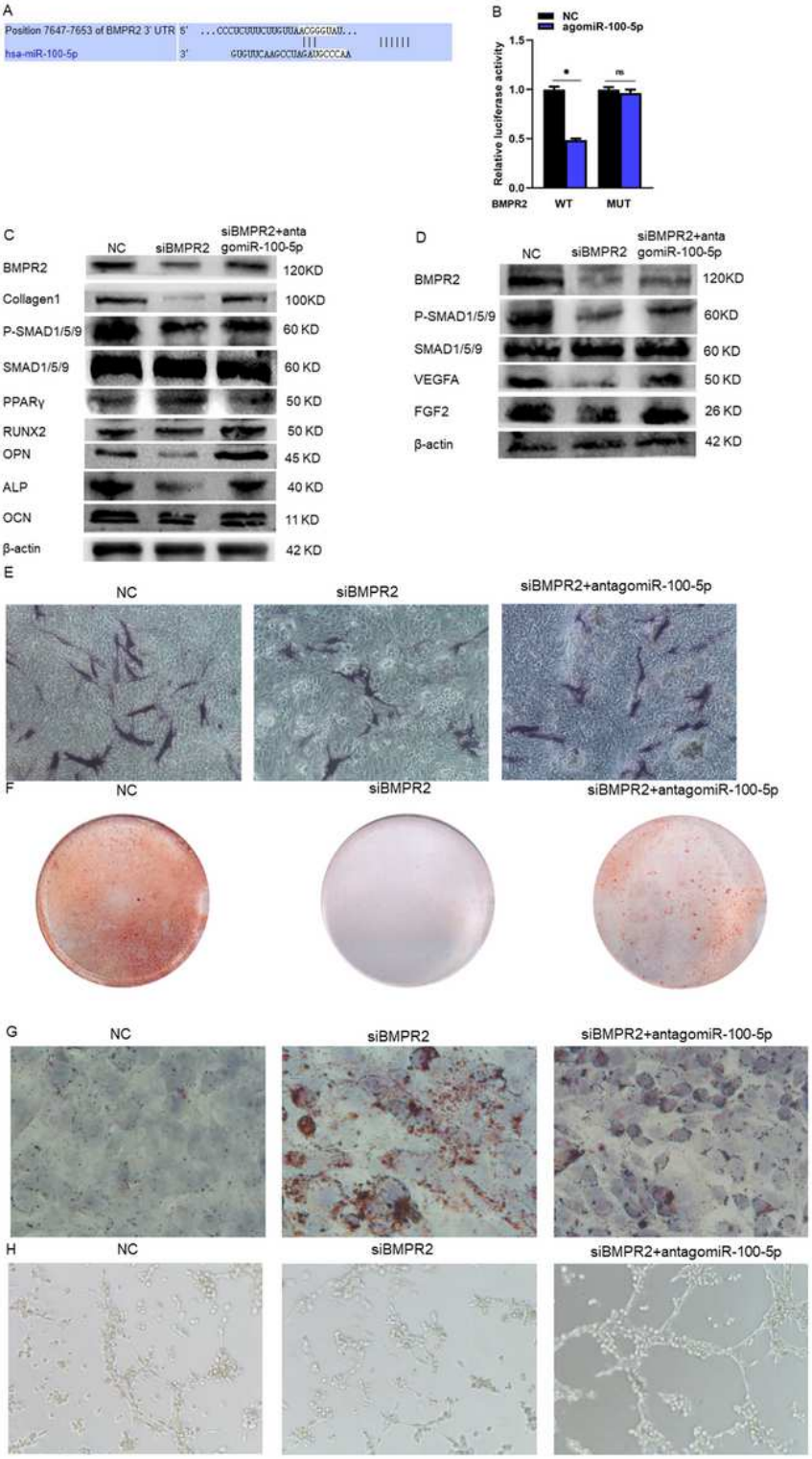

Figure 7

MiR-100-5p inhibits osteogenesis of BMSCs and angiogenesis of HUVECs by targeting BMPR2 and inhibiting BMPR2/smad1/5/9 pathway. A The target gene of miR-100-5p was predicted using Targetscan 7.2. B The targeting relationship between miR-100-5p and BMPR2 was verified by luciferase assay. C The expressions of Collagen1, BMPR2, SMAD1/5/9, p-SMAD1/5/9, OCN, RUNX2, ALP, OPN and PPARγ were measured using WB in BMSCs transfected with NC, siBMPR2 and siBMPR2+antagomiR-100-5p. D The

expressions of BMPR2, SMAD1/5/9, p-SMAD1/5/9, FGF2 and VEGFA were measured using WB in HUVECs transfected with NC, siBMPR2 and siBMPR2+antagomiR-100-5p. E ALP staining of BMSCs. (×100). F Alizarin red staining of BMSCs. G Oil red staining of BMSCs (×400). H Tube formation assay of HUVECs. *P <0.05, versus NC group; #P < 0.05, versus agomiR-100-5p group. All data were expressed as mean ± SEM.

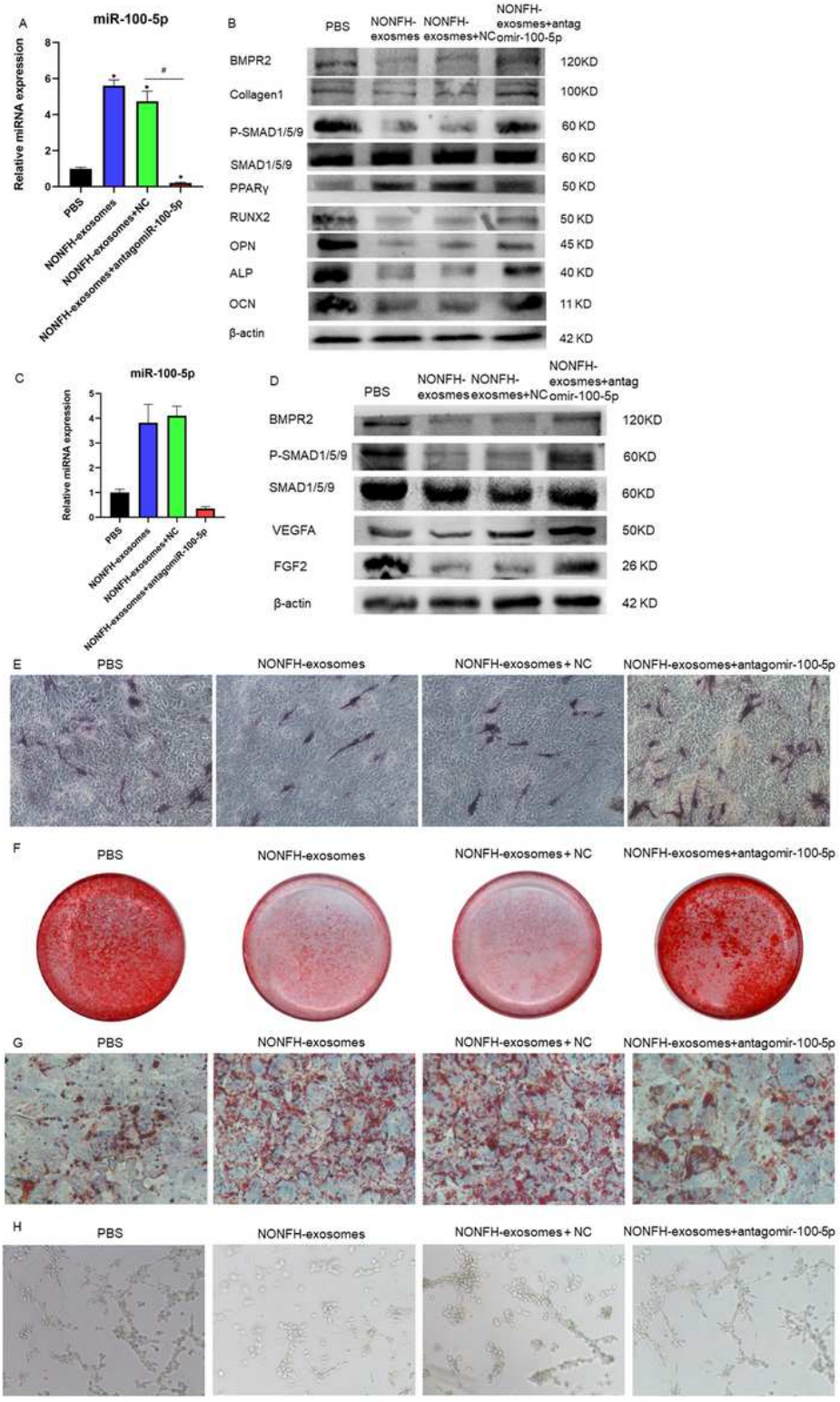

Figure 8

AntagomiR-100-5p rescued the suppression of osteogenesis of BMSCs and angiogenesis of HUVECs caused by NONFH-exosomes. A The expressions of miR-100-5p in BMSCs treated with PBS, NONFH-exosomes, NONFH-exosomes + NC and NONFH-exosomes + antagomir-100-5p. B The expressions of BMPR2, SMAD1/5/9, p-SMAD1/5/9, Collagen1, OCN, RUNX2, ALP, OPN and PPARγ were measured using WB in BMSCs. C The expressions of miR-100-5p in HUVECs treated with PBS, NONFH-exosomes, NONFH-exosomes + NC and NONFH-exosomes + antagomir-100-5p. D The expressions of BMPR2, BMPR2, SMAD1/5/9, p-SMAD1/5/9, FGF2 and VEGFA were measured using WB in HUVECs. E ALP staining of BMSCs (×100). F Alizarin red staining of BMSCs after cultured in ODM for 14 days. G Oil red staining of BMSCs (×400). H Tube formation assay of HUVECs. *P <0.05, versus NC group; #P < 0.05, versus agomiR-100-5p group. All data were expressed as mean ± SEM.